Gaussian Copula-based Bayesian network approach for characterizing spatial variability in aging steel bridges

Barros, B.; Conde, B.; Riveiro, B.; Morales-Nápoles, O.

DOI
10.1016/j.strusafe.2023.102403

Publication date
2023

Document Version
Final published version

Published in
Structural Safety

Structural Safety 106 (2024) 102403

Contents lists available at ScienceDirect

Structural Safety

journal homepage: www.elsevier.com/locate/strusafe

Gaussian Copula-based Bayesian network approach for characterizing spatial variability in aging steel bridges

B. Barros [a,*], B. Conde [a], B. Riveiro [a], O. Morales-Nápoles [b]

[a] CINTECX, Universidade de Vigo, GeoTECH Group, Campus Universitario de Vigo, As Lagoas, Marcosende, 36310 Vigo, Spain
[b] Faculty of Civil Engineering and Geosciences, Delft University of Technology, P.O. Box 5, 2600 AA Delft, the Netherlands

ARTICLE INFO

Keywords:
Gaussian copula-based Bayesian network
Random field
FE modeling
Aging steel bridges

ABSTRACT

Finite Element (FE) modeling often requires unavoidable simplifications or assumptions due to a lack of experimental data, modeling complexity, or non-affordable computational cost. One such simplification is modeling corrosion phenomena or material properties, which are usually assumed to be uniform throughout the structure. However, e.g., corrosion has a local nature and severe consequences on the behavior of steel structures that should not be overlooked. To improve the current numerical modeling techniques in aging steel bridges, this paper proposes a Gaussian Copula-based Bayesian Network (GCBN) approach to model the spatial variability of structural element properties. Accordingly, a study of the automatic Bayesian network generation process is first conducted. Subsequently, the methodology is applied to a severely damaged riveted steel bridge built in 1897. The results show that the methodology has excellent flexibility for generating properties variability in FE models at a low computational cost, thus ensuring its practical feasibility and robustness for accurate numerical modeling.

1. Introduction

Finite element (FE) modeling is a powerful tool that can support, facilitate, and make more robust the various tasks that need to be addressed throughout the service life of a bridge, such as preservation, maintenance, damage prediction, or reliability-based structural safety assessment [1]. Adequate FE modeling requires extensive experimental campaigns that can provide all the necessary data [2–4]. Nonetheless, model accuracy might be affected by simplifications or assumptions made through the modeling process, many of which are unavoidable [5]. Some of these issues are linked to aging or damage to the structure, which causes a reduction in strength and changes in the behavior of the members and connections that make up the bridge [6]. As was stated in [7], collapses due to deterioration account for around 25 % of truss-type bridge collapses.

In modeling steel bridges, a common simplification is to define corrosion only as a global and uniform phenomenon when it is also a process with a local nature, such as pitting [8]. Another common simplification is assuming all structural components have the same material properties. However, although the structure is generally made of the same material -and ignoring heterogeneities caused by the manufacturing process - the bridge elements do not exhibit the same behavior throughout the structure. This is due to some factors such as the corrosion state of the connections, the members' net section (i.e., the effective thickness), or stress concentration effects, among others, which cause a reduction in strength and severe changes in their behavior [9–11]. In recently built and undamaged bridges, the behavior of the different elements is more homogeneous, and the simplifications made in the modeling process can be considered appropriate since the actual behavior of the structure may not differ significantly (although model updating techniques are still recommended to reduce the gap between reality and computer simulation [12,13]). However, in damaged or aging bridges, these changes can lead to significant differences that should not be overlooked.

Among the different procedures for modeling the spatial variability and inhomogeneity of properties, random fields have been one of the main techniques in the last decades, with a significant increase in the number of works since 1990 until now. They have been widely used in various fields of study, such as fluid properties, turbulent flows, image segmentation or generation, earthquakes, or structural materials [14]. In the civil engineering field, several works have been developed that use random fields to represent the spatial variability of various properties and materials, such as laminated composite panels [15,16], spatial variations of material properties in tunnels [17,18], elastic moduli of

* Corresponding author.
E-mail address: brais.barros.gonzalez@uvigo.gal (B. Barros).

https://doi.org/10.1016/j.strusafe.2023.102403
Received 21 March 2023; Received in revised form 25 October 2023; Accepted 26 October 2023
Available online 6 November 2023

pavement layers [19], concrete material [20–22], corrosion distribution in reinforced concrete structures [23–25], or metal foam core sandwich material properties [26], wood or timber specimens [27,28]. For steel properties, random fields have also been extensively used in several works, such as [29], where pitting corrosion was modeled using random fields, or [30] and [31], where corrosion degradation modeling of steel plate specimens was studied.

Despite the significant development and increase in popularity of random fields, they typically have the disadvantage of being defined by a covariance or correlation length that may be sufficient to define continuous media. However, their robustness may be compromised when modeling the dependencies of discrete elements, such as the structural components of a bridge. In these cases, the connections between the elements and their characteristics have more influence on their properties than their distance in the structure. Bayesian Networks (BNs) are powerful tools for modeling structures with complex dependencies that can provide robust results. BNs are probabilistic graphical models that provide a joint distribution of interrelated random variables. BNs also have the advantage that, once modeled, they can predict new data using inference. For this reason, in addition to their high versatility and excellent performance in dealing with uncertainty quantification problems, they have become very popular in various fields of study.

In the field of civil engineering, BNs have been used for various purposes, such as the prediction of corrosion depth on buried pipelines [32], optimal inspection and maintenance planning for deteriorating structural components [33], data fusion of multiple sources for bridge assessment [34], sensitivity analysis [35], bridge scour risk assessment [36], reliability analysis of steel structures subjected to fatigue [37], reliability assessment of RC structures [38], for the multi-hazard fragility assessment of bridge systems [39] or optimal inspection strategies for structural systems [40] among others. Specifically, in the field of bridge engineering, several works with different objectives can also be found, such as residual strength prediction in an RC bridge [41], fatigue damage assessment in a steel deck [42], fatigue crack propagation modeling [43], or structural reliability prediction of a steel bridge element [44], among others. In the works mentioned above, several methodologies of BNs have been carried out; for an in-depth review, the reader is referred to [45] and [46]. Among the different types of BNs, the Gaussian Copula-based Bayesian Network (GCBN) has gained great popularity. The main advantage of using the Gaussian copula in the developed framework is its computational efficiency. This is the main reason for using the Gaussian copula implementation in [47–49]. Smaller models can be quantified using different copula families in which case a possibility would be to use vine copulas using the database Chimera [50]. Note, however that the number of models on up to 8 nodes is larger than 660 million. If only 8 nodes are sufficient to express variability in a particular application, then vine copulas parametrized using Chimera become a very attractive option to explore non-Gaussian dependence. In this case however hundreds of nodes are employed to represent spatial variability. The GCBN has demonstrated its versatility and robustness for modeling complex dependencies in several works, such as hurricane flood risk [51], reliability analysis of flood defenses [52], estimation of monthly maximum river discharge [53], or estimation of hydrodynamic forces on a submerged floating tunnel [54]. Several works have also been carried out in the bridge field, from developing a maintenance decision model for steel bridges [55] to the reliability analysis of reinforced concrete bridge columns [56]. Moreover, GCBN has proven to be very effective in modeling very high-dimensional problems, such as the works [57] and [58], where GCBN was used to model multi-variable weight-in-motion data.

GCBN has proven its efficiency in high dimensional problems, and its robustness in modeling complex dependencies with a low computational cost. For this reason, this work proposes the use of GCBN to model the spatial geometric and material properties variability in aging steel bridges. This paper focuses on the assessment of the variability generation process. However, It is worth mentioning that the practical implementation of this methodology (to model a specific structure using the proposed approach) requires additional research in which a framework is needed to select and optimize the parameters of the Bayesian network using experimental data. This methodology automatically analyzes the dependencies between the bridge structural elements and builds the corresponding Bayesian network. A comprehensive study of the influence of the controllable parameters in the automatic Bayesian network generation process has also been carried out. To implement the methodology, a refined FE model was developed with multiple partitions, each of which is a Bayesian network variable (879 variables). This results in a probabilistic FE model that avoids the usual simplifications in steel bridge modeling and provides more robust results. The feasibility of the methodology has been validated in a full-scale riveted steel bridge in Vilagarcía de Arousa, Galicia, Spain.

2. Gaussian copula-based Bayesian network

Bayesian networks (BNs) are graphical probabilistic models based on Directed Acyclic Graphs (DAG), where the nodes represent the random variables and the arcs represent the probabilistic dependencies between the linked variables [59]. The nodes connected by an arc follow the parent–child nomenclature, where the parent is the predecessor of the child node. A BN encodes the probability density function of a set of variables $\boldsymbol{X} = \{X_1, \cdots, X_n\}$ through the (conditional) independence statements established in the DAG and associated with a set of probability functions [57]. The d-separation principle establishes the criteria for interpreting (conditional) independence statements in the graphical model. The criteria focus around the three possible network connections denominated chain, fork and collider connections [60]:

1. Chain connections $(X_1 \rightarrow X_2 \rightarrow X_3)$: Chain connection entails that X_1 influences X_2 and X_2 influences X_3. This means that X_1 is not marginally independent of $X_3 (X_1 not \perp X_3)$. However, X_1 and X_3 are conditionally independent given $X_2 (X_1 \perp X_3 \,|\, X_2)$.
2. Fork connections $(X_1 \leftarrow X_2 \rightarrow X_3)$: Influence can pass between all the children of X_2 unless the state of X_2 is known. This means as in the chain connection that X_1 is not marginally independent of $X_3 (X_1 not \perp X_3)$ and X_1 and X_3 are conditionally independent given $X_2 (X_1 \perp X_3 \,|\, X_2)$.
3. Collider connections $(X_1 \rightarrow X_2 \leftarrow X_3)$: In this connection X_1 and X_3 influence X_2, i.e., X_1 is marginally independent of X_3 $(X_1 \perp X_3)$. They are however dependent given X_2 $(X_1 not \perp X_3 \,|\, X_2)$.

For an overview of the semantics used in BNs, the reader is referred to [59–61], and for a general overview of their applications, the reader is referred to [46,45]. Most applications of BNs focus on the representation of discrete random variables. This type of representation is inadequate for many problems and has several limitations [47]. The BNs that deal with discrete and continuous domains are called hybrid Bayesian networks (HBNs). Among the different methods of HBNs, conditional Gaussian models [62,63], dynamic discretization methods [64], variational approaches [65], and mixtures of truncated basis functions (MoTBFs) [66] can be mentioned, among others. A detailed review of HBNs, highlighting the advantages and disadvantages of each approach, is given in [67].

Gaussian Copula-based Bayesian Networks (GCBN) are HBNs constructing a multivariate joint distribution of a set of variables. For this purpose, GCBN associates nodes with random variables and arcs with bivariate pieces of dependence using a one-parameter conditional copula [68], thus defining the DAG dependence structure. The copula C is the function that describes the joint distribution $F_{X_i,X_j}(x,y)$ of two random variables X_i and X_j for $i \neq j$ as stated in Eq. (1).

$$F_{X_i,X_j}(x,y) = C_\theta \left[F_{X_i}(X_i), F_{X_j}\left(X_j\right) \right] \tag{1}$$

where θ is the parameter vector that provides the association measure between both random variables, such as the rank correlation (r). This describes the strength of the monotonic relation between the variables. The rank correlation of two random variables X_i and X_j with cumulative distribution functions F_{X_i} and F_{X_j} is calculated following Eq. (2).

$$r(X_i, X_j) = \rho\left[F_{X_i}(X_i), F_{X_j}(X_j)\right] \tag{2}$$

where ρ is the product-moment correlation of the random variables and can be computed through the variances and the expectations of X_i and X_j; see Eq. (3).

$$\rho(X_i, X_j) = \frac{E(X_i, X_j) - E(X_i)E(X_j)}{\sqrt{var(X_i)var(X_j)}} \tag{3}$$

The rank correlation can also be obtained using one parameter copulas as described in its population version, Eq. (4) [69].

$$r(X_i, X_j) = 12\int_0^1\int_0^1 C_\theta(u, v)dudv - 3 \tag{4}$$

where u and v are the margins of the one-parameter bivariate copula C_θ.

The GCBN methodology was initially developed in [70], stating that any copula with the zero-independence property can be used, i.e., zero correlation implies independence. However, as stated in [47], only the joint normal copula provides the advantage of fast computation/inference in large and complex problems. For this reason, GCBN was subsequently extended in [71], where normal copulas are used to realize the dependence structure specified via (conditional) rank correlations. The Gaussian copula uses the product-moment correlation (ρ) as a parameter, as shown in Eq. (5).

$$C_\rho(u, v) = \Phi_\rho\left[\Phi^{-1}(u), \Phi^{-1}(v)\right]$$

$$(u, v) \in [0, 1]^2 \tag{5}$$

where Φ_ρ is the bivariate standard normal cumulative distribution function and Φ^{-1} the inverse of the one-dimensional standard normal distribution function. The relationship between product-moment correlation (ρ) and rank correlation (r) using Pearson's transformation is described in Eq. (6) [72].

$$\rho(X, Y) = 2sin\left(\frac{\pi}{6} \bullet r(X, Y)\right) \tag{6}$$

Following Eq. (6), conditional rank correlations for normal copulas can be expressed as partial correlations. The conditional correlation of X and Y given $Z_1 = z_1, \cdots, Z_m = z_m$ is the one computed with the random vector $\left(\widetilde{X}, \widetilde{Y}\right)$ where $\widetilde{X}, \widetilde{Y}$ have the distribution of X and Y given $Z_1 = z_1, \cdots, Z_m = z_m$. The conditional rank correlations are computed with the ranks of $\left(\widetilde{X}, \widetilde{Y}\right)$. In normal copulas, partial correlations are equal to conditional correlations (because the joint copula can be transformed to a joint normal distribution) and can be computed recursively following Eq. (7) [73] where m denotes the number of parents $Pa_j(X_i)$ for the node X_i.

$$\rho_{1,2;3,\cdots,m} = \frac{\rho_{1,2;4,\cdots,m} - \left(\rho_{1,3;4,\cdots,m}\right)\left(\rho_{2,3;4,\cdots,m}\right)}{\sqrt{(1 - \rho^2_{1,3;4,\cdots,m})(1 - \rho^2_{2,3;4,\cdots,m})}} \tag{7}$$

Considering a BN on n variables, the joint distribution satisfies the characteristic of factorizations as described in Eq. (8) where $f_{1,\ldots,n}$ denotes the joint density of the n variables, f_i their marginal densities and $f_{i|Pa(i)}$ the conditional densities [47].

$$f_{1,\ldots,n}(x_1, \ldots, x_n) = f_1(x_1)\prod_{i=2}^{n} f_{i|Pa(i)}\left(x_i|x_{Pa(i)}\right) \tag{8}$$

Each variable X_i is represented by the node i. The arch that joins the parent node with the child node $Pa_j(X_i) \rightarrow X_i$ is associated with the conditional rank correlation as described in Eq. (9) where the index j is in the non-unique order, i.e., the order of the parents can be permuted.

$$\mathrm{r}\left(X_i,\ Pa_j(X_i)\right), \begin{cases} \mathrm{j} = 1 \\ \mathrm{j} = 2, \ldots, m \end{cases} \quad r\left(X_i,\ Pa_j(X_i)|Pa_1(X_i), \ldots, Pa_{j-1}(X_i)\right), \tag{9}$$

these assignments are algebraically independent and they uniquely determine the joint distribution for a particular choice of copula as states the following theorem:

Theorem 2.1. *Given:*

1. *A DAG with n nodes specifying conditional independence relationships;*
2. *n variables* $X_1, \cdots, X_n$, *assigned to the node with invertible distribution functions* $F_1, \cdots, F_n$;
3. *The specification stated in* Eq. (8), $i = 1, \cdots, n$, *of conditional rank correlations on the arcs of the GCBN;*
4. *A copula realizing all correlations [-1,1] for which correlation 0 entails independence.*

the joint distribution of the n variables is uniquely determined. This joint distribution satisfies the characteristic factorization (Eq. (8)) *and the conditional rank correlations in* (Eq. (9)) *are algebraically independent.*

However, a modification of this theorem was proposed (Theorem 2.2) to allow for various types of copulas. If the conditional independence statements were not specified as zero rank correlations, but as (conditional) independent copulas, then the (conditional) rank correlations associated with the arcs could be realized by any copula that realizes all correlations [-1; 1]. For instance, an GCBN could be quantified with a mixture of (conditional) independent copulas and t-copulas. The possibility of using the multivariate t-copula, with different tail dependence for each pair of (conditional) variables allows to capture dependent extreme values [47].

Theorem 2.2. *Given:*

1. *A DAG with n nodes specifying conditional independence relationships;*
2. *n variables* $X_1, \cdots, X_n$, *assigned to the node with invertible distribution functions* $F_1, \cdots, F_n$;
3. *The specification stated in* Eq. (8), $i = 1, \cdots, n$, *of conditional rank correlations on the arcs of the GCBN;*
4. *A copula realizing all correlations [-1,1];*
5. *The (conditional) independent copula realizing all (conditional) independence relationships encoded by the graph of the GCBN;*

the joint distribution of the n variables is uniquely determined. This joint distribution satisfies the characteristic factorization (Eq. (8)) *and the conditional rank correlations in* (Eq. (9)) *are algebraically independent.*

Finally, marginal distributions and arbitrary (conditional) copulas need to be specified in order to quantify GCBN. The marginal distributions can be obtained from data or experts [74] or using the empirical marginal distribution fitting parametric forms. The (conditional) copulas are parametrized by (conditional) rank correlations that can be calculated experimentally from data or provided from experts [75]. Besides, it is generally not mandatory to set the conditional rank correlations as constant but they are usually assumed constant for convenience [47]. Each arc between a parent and a child is associated to a conditional rank correlation. In the case where a child has multiple parents, the order of these parents can be non-uniquely determined. When experts contribute to constructing the structure of the GCBN, they

can determine an order for the parents based on their decreasing influence on the child. Alternatively, the order of the parents may be determined by data availability or another criterion. It is important to note that there is no singular procedure or criterion to construct the directed acyclic graph (DAG) of the GCBN.

The methodology described in this section has been implemented in BANSHEE, an open-access scriptable code developed as a toolbox in MATLAB [48] and Python [49]. For this study, the MATLAB version of BANSHEE was employed. This toolbox allows the quantification of the BN, the validation of the underlying assumptions, the visualization of the network and its corresponding rank correlation matrix, and finally, the computation of inference with a BN based on existing or new evidence.

3. Paraíso bridge

The structure used to demonstrate the applicability of the proposed methodology is a riveted steel bridge that crosses the Umia River near the village of Paraíso in Galicia, Spain. It was part of the old railway line that connected the cities of Pontevedra and Vilagarcía de Arousa. It was built in 1897 and was in service until 2008. In 2020 it was refurbished and is now part of a greenway open to pedestrians and cyclists. The main views of the Paraiso bridge are shown in Fig. 1.

The central span has a total length of 37.0 m, a width of 2.6 m, and a height of 4.1 m. The bridge is composed of 4 primary chords that form a trapezoidal box, 52 diagonal beams reinforcing this box (type I and II), 24 verticals, 15 torsional bracings, 12 lower and 12 upper lateral bracings and 15 transverse bracings. In the upper part of the deck, there is a frame composed of 2 stringers that cover the length of the bridge, reinforced by 15 cross-girders. In addition, the stringers are reinforced by 12 lateral and 12 X-shaped bracings. The main dimensions of the bridge and the structural members are shown in Fig. 2.

After a comprehensive inspection of all bridge elements, many were found to be in an advanced state of corrosion. The plates and angles that make up the beam profiles are among the most damaged elements. In addition, some steel connections are severely damaged, see Fig. 3. The chord webs also show relatively high levels of generalized corrosion, with degradation and delamination of the angles connecting the web to the flanges (Fig. 3). The degree of corrosion of these elements can be partly explained by their arrangement, which leads to water accumulation during rainy periods, thus increasing the corrosion progress.

4. FE modelling

As an initial stage of the modelling process, the geometrical characterization was carried out with the aid of a digital gauge with an accuracy of $\pm$ 0.01 mm. Eleven profiles with different cross-section were identified along the entire structure (See Fig. 2). Some of these profiles are reinforced depending on their location. For instance, the chords, which are reinforced with two or even three steel plates in the central areas, or the verticals or the type 1 diagonals, which are reinforced towards the ends of the structure. As a result of the geometrical characterization, the measurements of all the profiles that constitute the bridge were obtained and schematized in a CAD model using Ansys Spaceclaim Software [76]. It should be noted that a great variability has been identified in the measurements taken due to the high level of corrosion in the structure. For this reason, nominal measurements were defined for the profiles that symbolize the average value obtained for the different measurements taken on the same element in different parts of the structure. The dimensions of the main components that form the bridge are described in Fig. 4.

Based on the geometric characterization performed, the finite element (FE) model of the structure was developed. First the boundary conditions were defined. Simple supports were implemented in one side of the bridge and roller supports in the other side, as observed during the geometric characterization process. In both cases in-plane (Z-axis) rotations were allowed and, in case of the roller supports, the longitudinal displacements were also allowed (X-axis). Then, the modeling process of the bridge was performed using line bodies in the Diana FEA software [77]. The main structural members of the bridge were defined as two-node three-dimensional Class I beam elements. On the other hand, the bracings were modeled as two-node directly integrated truss elements.

Fig. 1. Main views of the Paraíso bridge.

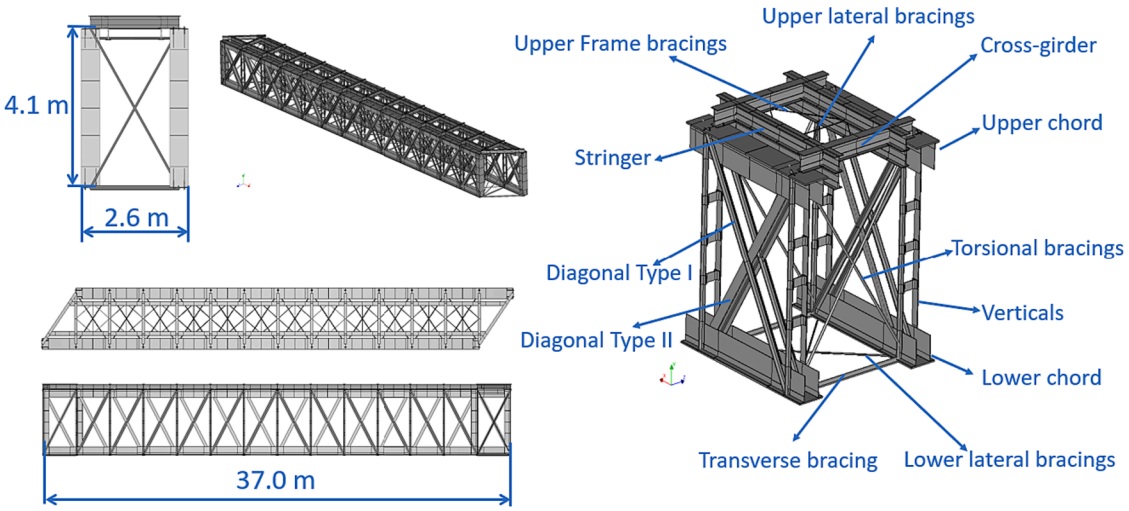

Fig. 2. Outline of the structural members and main dimensions of the Paraíso bridge.

Fig. 3. Detail of corroded elements in the Paraiso bridge a) chord web b) gusset plates at the connection between stringers and cross-girders c) connection of the lower lateral bracings to the chords.

The cross-sections that make up the bridge are formed by riveted steel shells that form complex and irregular geometries. Since these are non-standardized cross-sections, they must be entered in Diana FEA as *"arbitrary shapes"*, which consists of entering the cross-section geometry by means of coordinates. To define the coordinates of the cross section, the profile must be subdivided into zones composed of 4 points. The set of the different zones will define the cross-section shape. In order to parameterize the thicknesses and to vary them automatically, an algorithm has been developed using MATLAB software [78]. This algorithm recalculates the coordinates of the different zones according to the corrosion of each plate and the centroid of the overall cross section (the set of the different zones). It also recalculates the eccentricities assigned to each profile according to its corrosion. Finally, the algorithm is programmed to automatically enter the new profiles in the Diana FEA software exporting the model to "*.dat*" extension in order to introduce the new profiles, following the *"batch syntax"* defined in Diana's manual for *"arbitrary shapes"*.

A mesh size of one division per element was used for the model. A single division was implemented because each chord was separated into several different geometric elements (line bodies) to discretize further the bridge and its components around the steel connections. Thus, a division was implemented at a distance of 0.5 m from each node. In addition, the line bodies were further subdivided to represent the different reinforcements (see Fig. 5) that some beams contain, such as the chords and verticals, further increasing the number of subdivisions. By implementing these subdivisions, the model was expanded from the original 278 line bodies to a total of 879 line bodies. For this reason, and in order to find a balance between accuracy and computational cost, it

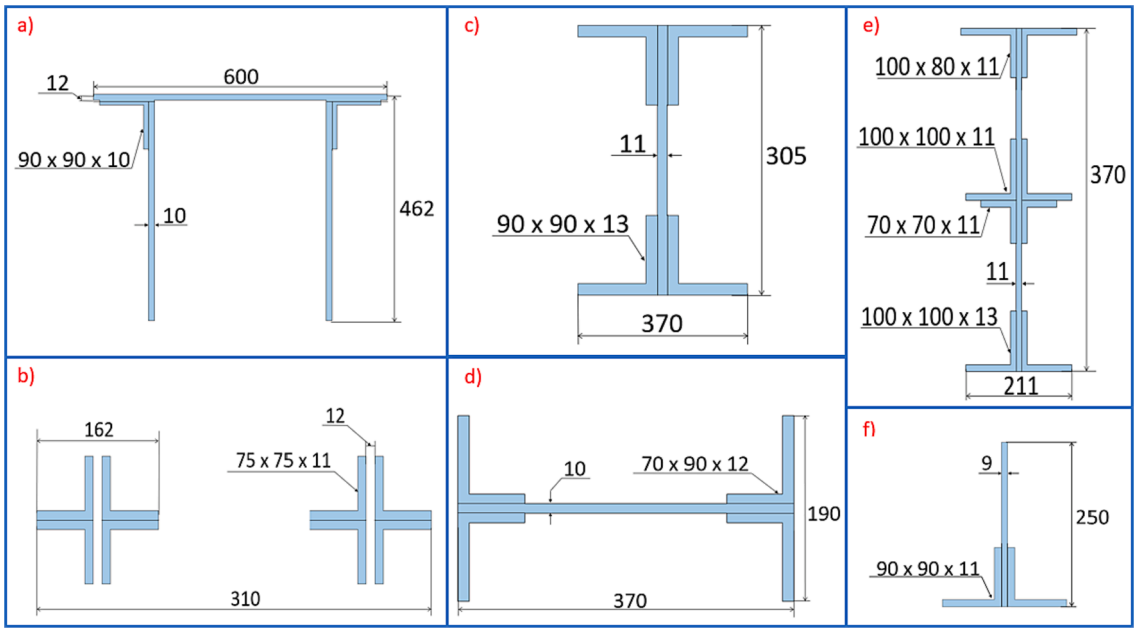

Fig. 4. Main dimensions in mm of the profiles of Paraíso bridge: a) Chords, b) Verticals and diagonals type I, c) Cross-girder, d) Diagonal beam type II, e) Stringers, f) Transverse bracings.

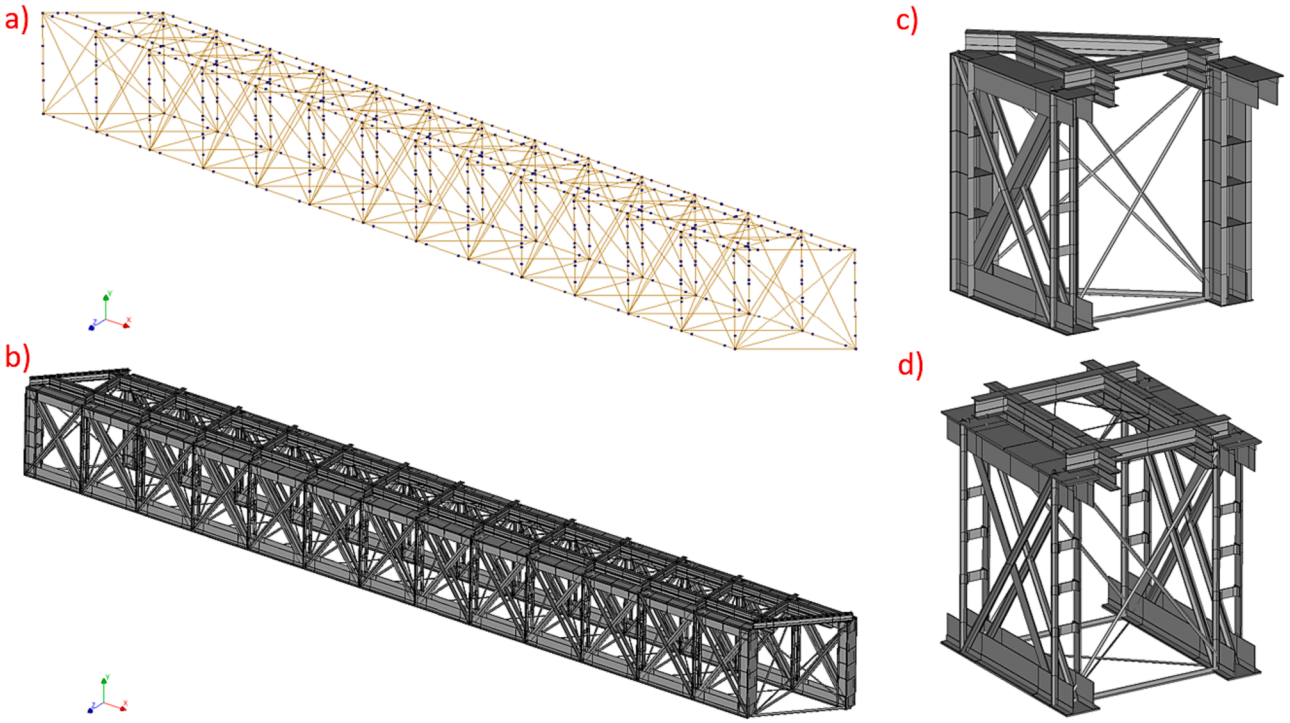

Fig. 5. FE model of the Paraíso bridge a) geometrical model based on line bodies b) FE model with the profiles' cross sections c) detail of the end section of the model d) detail of a middle section of the model.

was decided that a single division per element would be sufficient.

As model input variables, the thickness variations of the structural members and the steel material properties were considered. Initially, it was decided to define uniform distributions for all variables because normal distributions can produce unrealistic values such as thickness variations greater than the original thickness. In addition, future work will use sensitivity analysis techniques prior to model calibration. In sensitivity analysis techniques it is beneficial to use uniform distributions to explore the sample space equally. In this work, the bounds chosen are not a crucial aspect to demonstrate the viability of the proposed methodology and were established as an example in order to represent realistic values. The range of thickness variation for the different elements was established as a nominal measure $\pm$ 2.0 mm, where the nominal measure is the rounded average measured thickness and 2.0 mm is the maximum theoretical thickness reduction obtained according to the current European standards of corrosion in metals [79,80,80] for a corrosivity category of C4 and given the age of the bridge. Regarding the material properties, the lower and upper bounds of the density were obtained using the three sigma rule of

thumb (99.7 % confidence interval) in the distribution recommended in the JCSS probabilistic model code which follows a normal distribution with a mean of 7850 Kg/m^3 and a coefficient of variation (CoV) of 1.0 % [81]. For the elastic properties, to represent the corrosion-induced effects, the lower limit of Young's modulus was obtained based on a 99.7 % confidence interval for a log-normal distribution with a mean of 200 N/mm2 and a CoV of 5 % [82,83], and the upper limit was obtained according to the value established for structural steel in the Eurocode [84]. The upper limit follows a different criterion from the lower limit because, had they used the same criterion, the value obtained (230 N/mm^2) would have been unrealistic for aging steel.

Finally, a second algorithm was developed in Python that classifies all bridge elements by profile type, location, and corresponding nodes. The code then creates a copy of the original FE model and defines a material and an element geometry property for each bridge element. This code is designed to discretize and apply different geometric and material properties to the different elements of the bridge in a fully automated way.

5. Spatial variability characterization through GCBN

As introduced earlier, random fields are valuable tools for modeling spatial variability. However, in the case of inhomogeneous (for example negative correlations in space appearing together with positive ones), "discrete" space dependence, and complex dependence structures in general, their ability to reproduce the dependence of elements is quite limited. Bayesian networks are probabilistic graphical models that provide a joint distribution of a large number of interrelated variables, i.e., they can represent complex dependency structures. In this study, Bayesian networks were used to define the dependencies of the elements that make up the FE model of the Paraiso bridge and to generate spatial variability in the desired model input variables.

5.1. Framework

As a first step, the directed acyclic graph (DAG) of the Bayesian network was defined. In this framework, each node of the DAG represents one structural element of the FE model of the bridge (879 structural elements in total). Each node of the Bayesian network contains the probability distribution of the variable for which the spatial variability wants to be generated. According to the approach adopted in the framework, a Bayesian network can only generate variability in a single variable of the model. To generate variability in independent variables (uncorrelated with each other), as many BNs as variables are needed and the DAG of each BN will be formed by as many BN nodes as structural elements in the FE model. In the case of correlated variables, the algorithm must be reconfigured to generate for each structural element as many BN nodes as desired variables. To correlate both variables it is only necessary to join both nodes by means of an arc and specify a value of conditional rank correlation. This is another great advantage over the random fields, since in these, correlating variables is not so straightforward. The Gaussian copula-based Bayesian network is classified as "hybrid" and can handle both discrete and continuous variables although in this research we restrict ourselves to the purely continuous case. Therefore, this type of BN is suitable for all types of problems since it is very robust (see introduction section and references therein). In this case study, the random variables (thickness variation and Young's modulus) were considered as continuous and independents (both parameters are not correlated with each other). For this reason, two Bayesian networks were created to generate thickness and Young's modulus values for each bridge element.

To automatically generate the DAG, an algorithm was developed using MATLAB. This algorithm uses the exported version of the FE model with the extension ".dat" to determine how the different structural elements are connected and how they are arranged in the structure. For this purpose, the algorithm explores all the structure analyzing the mesh nodes that make up each structural element and defines a list of elements and their corresponding mesh nodes. The code has been configured to generate different DAG structures depending on the structural elements selected as initial points (nodes without parents). Therefore, the code will generate different BNs depending on the initial points selected. For this reason, the number of initial points (N) must be specified to execute the algorithm, and thus the code will randomly select N elements. Then the steps followed by the algorithm are explained below:

1. In the first iteration, the algorithm identifies the mesh nodes of the structural elements selected as initial points and creates the corresponding BN nodes.
2. Then the algorithm identifies the connected structural elements using the mesh nodes, i.e., those structural elements that share the same mesh node are the adjacent structural elements.
3. The algorithm creates the BN nodes of the adjacent elements.
4. The parent–child relationship of the Bayesian Network nodes representing the connected structural elements is defined.

Once the BN nodes of the initial points and their corresponding child nodes were created and their relationships were defined using arcs, the points 2, 3 and 4 are repeated until the algorithm does not detect any structural element that has not been previously selected. The workflow of the proposed methodology is summarized in Fig. 6.

An example of the DAG generated for a bridge section is shown in Fig. 8. At each iteration, connected elements are detected and classified as children of the Bayesian Network node under evaluation. The code continues until all elements of the structure have been classified and their parents have been assigned. Fig. 7 shows some steps of the evolution of the algorithm. Fig. 8 shows the DAG generated for this particular example.

The connection between two BN nodes is made by means of arcs that follow the parent–child direction. This direction depends on the initial

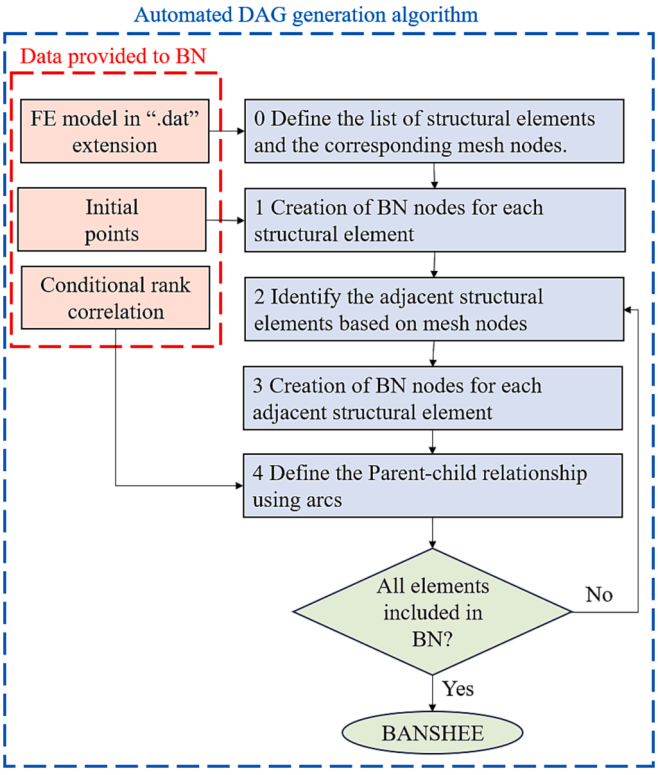

Fig. 6. Workflow of the developed algorithm to automatically generate de DAG of the Bayesian network.

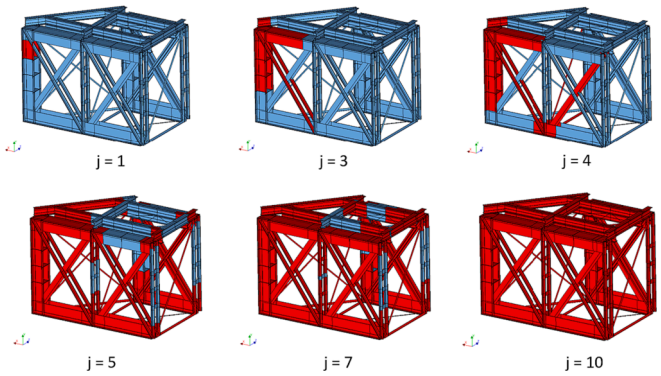

Fig. 7. Steps (j) of the classification algorithm exploring a subsection of the structure; the evaluated elements are highlighted in red. This example corresponds to a single realization of many implemented in this research. (For interpretation of the references to color in this figure legend, the reader is referred to the web version of this article.)

points chosen by the algorithm and affects the results, i.e., it is not the same for node 1 to depend on node 2 as node 2 to depend on node 1. However, since the problem is approached probabilistically, with hundreds or thousands of runs in each simulation, it can be said that both directions are considered when obtaining a final result. These arcs represent the bivariate pieces of dependence and are defined as the conditional rank correlations which should be provided to run the algorithm. Ideally, the conditional rank correlations should be obtained from measurements of the bridge properties. However, due to the high dimensionality of the problem (879 variables), a significant number of experimental measurements would be required to obtain an accurate value of the conditional rank correlations. For this reason, expert judgment is a common approach in this type of problems, to determine an appropriate value of the conditional rank correlation [85–88,75]. In this case study, the algorithm was designed to set the same value of the conditional rank correlation value between each pair of nodes. Following this approach, the variable conditional rank correlation represents the correlation between the variable of any pair of adjacent structural elements. With a minor reconfiguration of the code, other approaches could be implemented such as setting correlation values according to the connection type, the profile of the structural element, or its degree of exposure. However, this would require a high discretization of the conditional rank correlation. Since this framework was implemented to perform a calibration in a future work, it was initially preferred to lump all elements into a single correlation variable until a sensitivity analysis was performed. Once it was verified that the variable is sensitive in the FE model responses, an iterative process could begin in order to find the most accurate approach (if necessary) avoiding excessive discretization, which can lead to model responses becoming insensitive to the correlation variables.

Once the DAG structure is defined and the conditional rank correlation for the different arcs is fixed, the capabilities of BANSHEE [48] are exploited to construct the rank correlation matrix. BANSHEE builds a joint distribution coupling the marginal distributions of each node through the use of the Gaussian copula and with the dependence structure constructed from the bivariate pieces of dependence (arcs) for a selected value of the conditional rank correlation. In this study, all nodes are defined as variables following a beta probability distribution and with the bounds defined in Section 4. Once the joint distribution is constructed, and the distributions of each node are defined, the thickness and Young's modulus variability can be obtained for each bridge element. First, random samples are generated from a uniform marginal distribution [89]. Then, the values of thickness and Young's modulus variability are derived from the generated samples [90]. The algorithm uses a self-developed Python script to execute the Python commands predefined in the software Diana FEA to change the material and geometric properties for each structural element. To do this, the algorithm makes a copy of the FE model and automatically creates as many

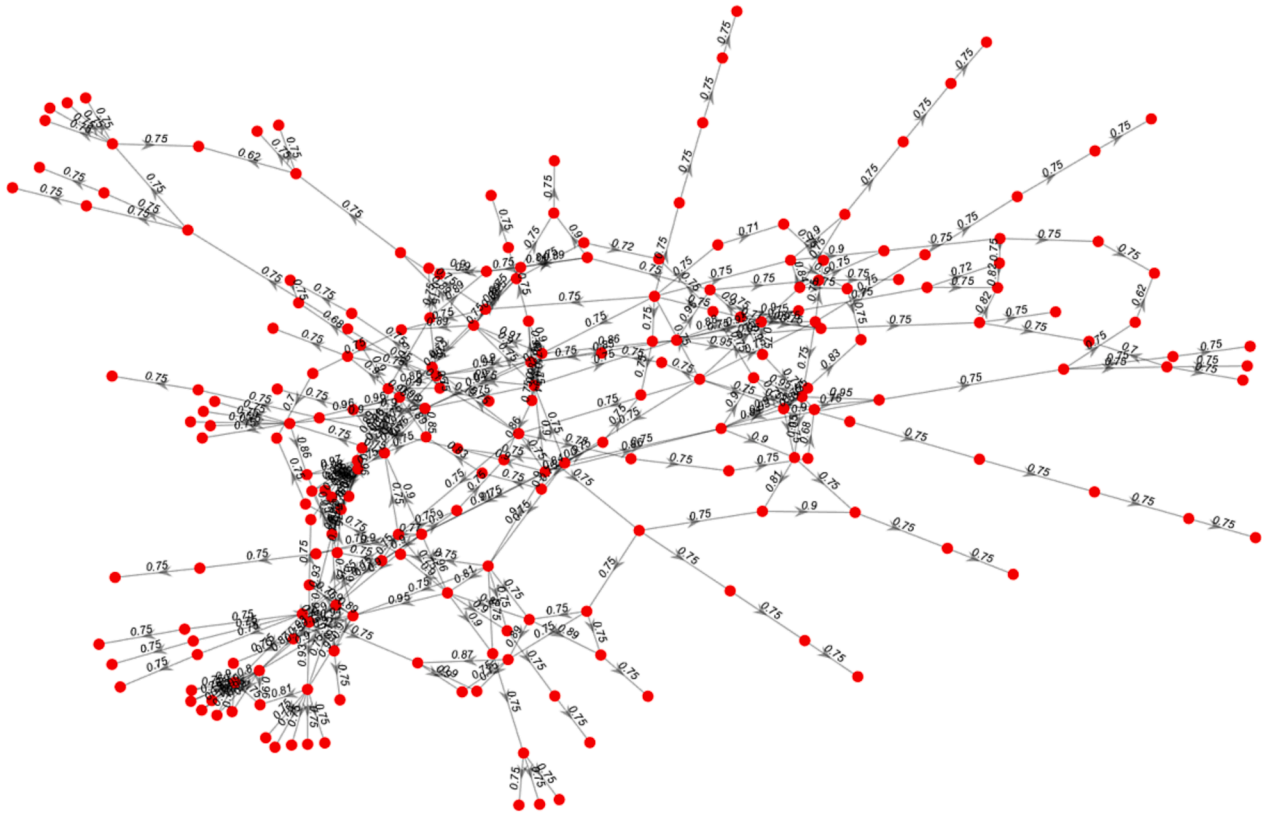

Fig. 8. Example of the DAG created for a subsection of the structure.

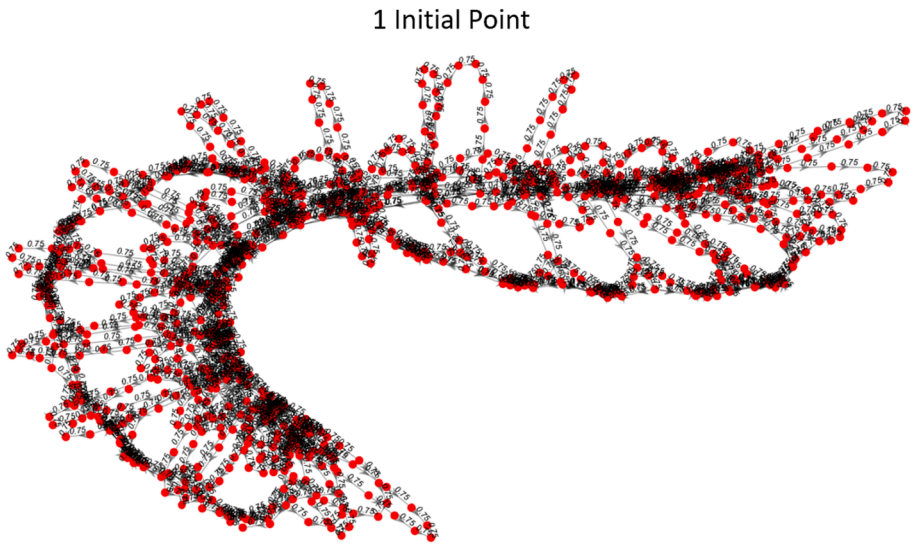

Fig. 9. Directed Acyclic graph (DAG) of a Bayesian network with one initial point.

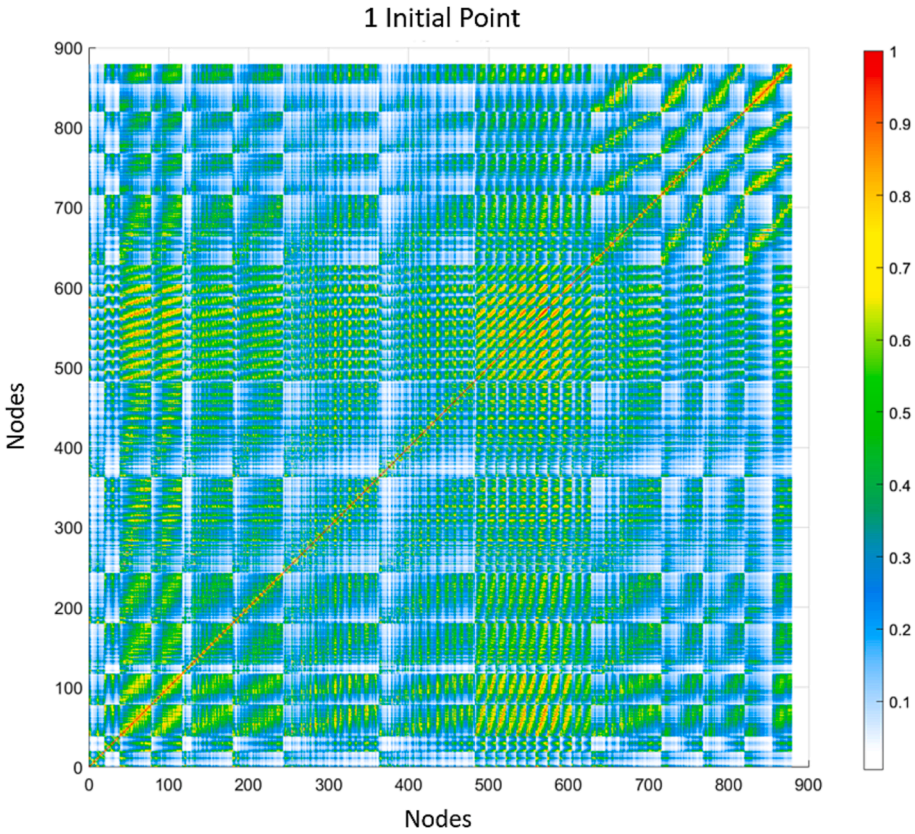

Fig. 10. Correlation matrix of a Bayesian network with one initial point.

materials and element geometries (cross-sections) as structural elements (the variation is applied uniformly to each element). Then, it substitutes the thickness and Young modulus values for each structural element. Moreover, the code also creates additional copies of the model in which a color scale represents the thickness and Young's modulus variability to visually evaluate the values generated (see Fig. 17).

Since the initial points and the conditional rank correlation have a strong influence on the automatically generated Bayesian network and thus on the generated variability, the study of the influence of these parameters was thoroughly addressed. A summary of the main results and conclusions of this study are presented in sections 5.2 Initial points and 5.3 Conditional rank correlation. The complete study of these parameters is included in a supplement available upon request to the corresponding author. As examples, the illustrations of the DAG (see Fig. 9) and the correlation matrix (see Fig. 10) are shown for the case of 1 initial point and a conditional rank correlation of 0.75 using the developed methodology.

5.2. *Initial points*

As mentioned in the previous section, the DAG is automatically generated in the developed methodology. The only required inputs are

Table 1
Mean number of arcs (μ) and standard deviation (σ) in 100 Bayesian networks with a different number of starting points.

Initial Points	1	2	5	10	25	50	100	150
μ	1771	1768	1766	1775	1816	1890	2043	2174
σ	11.17	13.49	14.07	16.00	17.88	18.87	17.13	17.26

the number of starting points and the conditional rank correlation between nodes. In order to understand how the initial points influence the Bayesian network, a total of 800 Bayesian networks with different starting points (1, 2, 5, 10, 25, 50, 100, 150) have been generated. Bayesian networks with more than 150 starting points have not been generated because they lead to the creation of correlation matrices very close to singularity. Besides, a constraint implemented in the developed algorithm makes each element selected as the initial node to be in a different bridge region. Since the starting points are chosen arbitrarily, it was decided to simulate 100 times each of the abovementioned combinations of starting points by setting the conditional rank correlation to 0.75 to analyze only the effect of the starting points without the influence of the conditional rank correlation. These 800 Bayesian networks generated with a conditional rank correlation of 0.75 are called "Positive cases". The DAGs obtained present similar structures, and their differences are not perceptible due to the large number of variables. However, the number of initial points creates a quite considerable saturation difference in the graph. Table 1 shows the average number of arcs (μ) obtained for the 100 Bayesian networks and its standard deviation (σ) for the different number of starting points. As can be seen, the network saturation increases with the number of starting points.

The increase in the number of starting points entails an increment in the number of independent points (nodes without parents) and the saturation of the DAG structure. These changes can be easily observed in the color maps representing the correlation matrix of the Bayesian Network. Such an increase provokes the initial blue or green areas to become white, as shown in Fig. 11. The part that remains invariant with high correlation values represents the correlations of adjacent or nearest elements in the structure, while the areas with lower values represent the correlations between the more distant elements. As the number of independent points (initial points) and the network saturation increases, the more distant elements tend more quickly to low or zero correlation values. In cases of higher saturation, as in the case of 150 starting points, only the elements very close in the structure will present correlation, leaving the remaining elements with practically null correlation. Therefore, it can be concluded that the number of starting points hardly affects the correlation between the closest or adjacent elements, but it does have severe consequences for the correlation values of the most distant elements.

To quantify how the multivariate Gaussian distributions are affected by the DAG structure, two techniques have been employed to quantify the difference between the correlation matrices. Due to the high number of variables that conform the network, the first technique is the symmetric KL (Kullback-Leibler) divergence technique [91], which measures the distance between two distributions. The second technique is the metric developed by Abou-Moustafa [92]. Both methods are ideal for problems with many variables since it does not use the matrix determinant. The symmetric KL divergence and Abou-Moustafa metrics are computed as stated in Eqs. (10) and (11), respectively:

$$d_{KL}(D_1,D_2)=\frac{1}{2}(\mathrm{m}_1-\mathrm{m}_2)^T\left(\mathrm{R}_1^{-1}-\mathrm{R}_2^{-1}\right)^T(\mathrm{m}_1-\mathrm{m}_2)+\frac{1}{2}tr\left(\mathrm{R}_1^{-1}\mathrm{R}_2+\mathrm{R}_2^{-1}\mathrm{R}_1-2I\right) \tag{10}$$

$$d_G(D_1,D_2)=\left((\mathrm{m}_1-\mathrm{m}_2)^T\left(\frac{1}{2}\mathrm{R}_1+\frac{1}{2}\mathrm{R}_2\right)^{-1}(\mathrm{m}_1-\mathrm{m}_2)\right)^{1/2}+\left(\sum_{k=1}^{n}log^2\lambda_k(\mathrm{R}_1,\mathrm{R}_2)\right)^{1/2} \tag{11}$$

where D_1 and D_2 are the multivariate Gaussian distributions to be compared, and m_1 and m_2 are the mean vectors of their respective covariance matrices (R_1 and R_2). In Eq. (11), λ_k represents the generalized eigenvalues for the generalized eigenvalue problem $\mathrm{R}_1 v=\lambda \mathrm{R}_2 v$.

Both techniques are composed of two terms, i) the difference between means and ii) the difference between covariance matrices. In this work, as the Gaussian copula was employed with a zero mean, the dissimilarity measures are reduced to the second term (covariance matrix differences). Herein, we present only the results obtained for the Abou-Moustafa metric. The results of both techniques are similar, although with some differences, such as the lower robustness of the symmetric KL divergence technique when the matrix is very close to the singularity.

Since the distance techniques employed are not standardized, a comparative analysis was made to study the variation range of their values. For this purpose, "Negative cases" and "Independent Case" were created to verify that the results of both techniques are robust. The "Negative cases" use the same DAG as the "Positive cases" but setting the conditional rank correlation to −0.75. The "Independent case" corresponds to the identity matrix, meaning each element is only correlated with itself. Fig. 12 shows, classified by the number of initial points, the average distances obtained for the following cases: a) "Positive cases" with themselves (in red), b) "Positive cases" with "Negative cases" (in blue), and c) "Positive cases" with "Independent case" (in green).

As can be observed, the distances obtained among the "Positive cases" are lower than the comparisons with the Negative and Independent cases. This fact entails that the metric presents a robust behavior, and the distances obtained are coherent. Besides, it can be noticed how the distances tend to increase with the number of initial points. This fact is more clearly illustrated in Fig. 13, which shows the cumulative density function for the distances obtained among the positive cases and classified according to the number of initial points. This is because a high number of initial points induce a high number of independent nodes, and since the initial points are randomly chosen, when the number of initial points increases, more different Bayesian networks are obtained.

Finally, the distances obtained among the 100 Bayesian networks with the same number of initial points were computed. Table 2 summarizes the mean and the standard deviation (σ) of the distances obtained. As can be seen, the elements selected as initial points provoke high differences between the Bayesian networks obtained. When the number of initial points increases, the differences between the Bayesian networks are further incremented. For this reason, it can be concluded that the number of initial nodes and the selection of the elements chosen as initial nodes provoke high differences in the resulting Bayesian network.

5.3. Conditional rank correlation

Once the influence of the initial points on the Bayesian networks was analyzed, the study of the conditional rank correlation was carried out. For this purpose, Bayesian networks with conditional rank correlation values (0.1, 0.25, 0.5, 0.6, 0.75, 0.9) were built for the cases of 1 and 150 initial points. Fig. 14 represents the color maps of the correlation matrices obtained for 1 initial point and the different conditional correlation values, and Fig. 15 for the case of 150 initial points.

In both cases, it can be noticed how the conditional rank correlation globally affects the correlation of the Bayesian network. For low values of conditional rank correlation, the correlation matrix presents very low

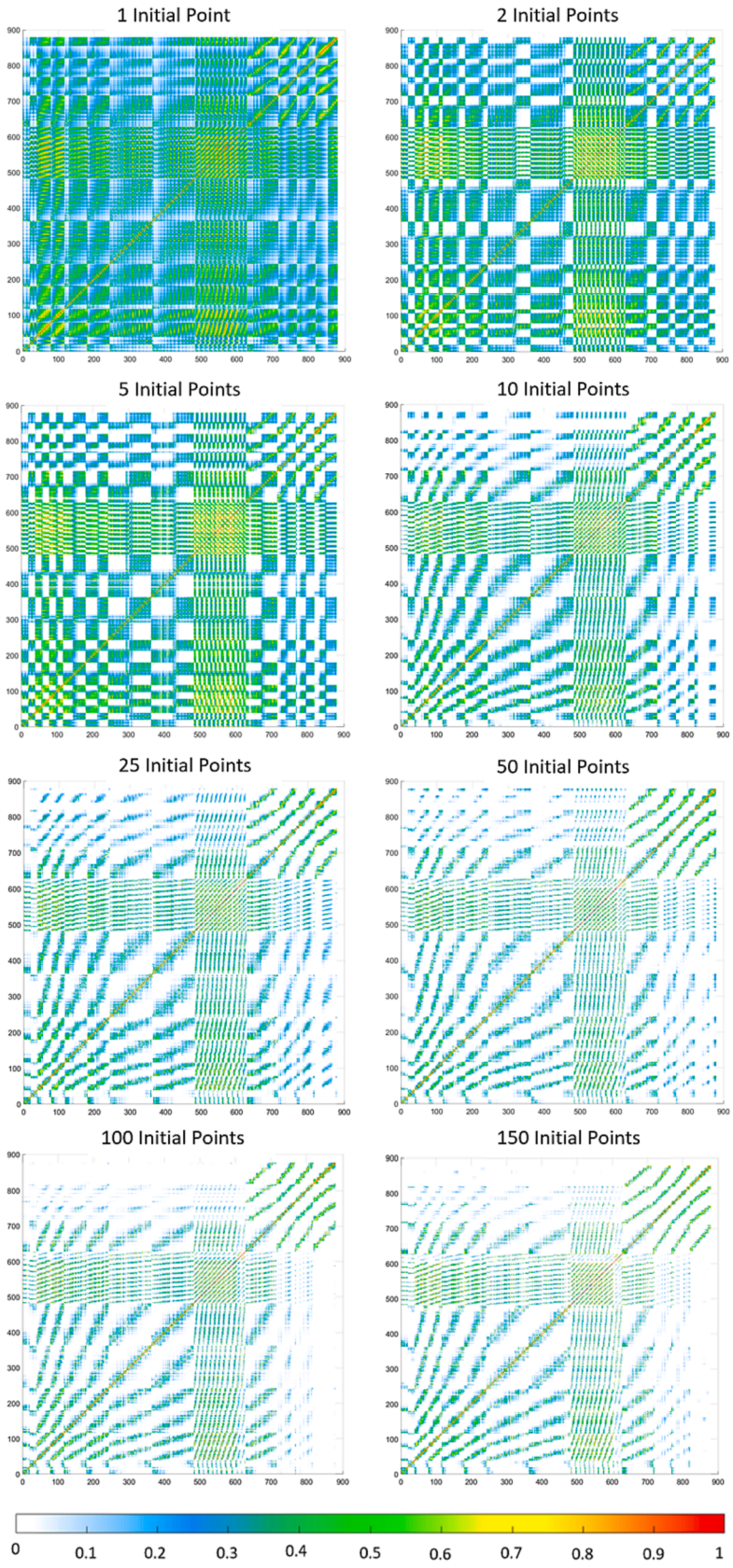

Fig. 11. Comparison of the correlation matrices regarding the number of initial points.

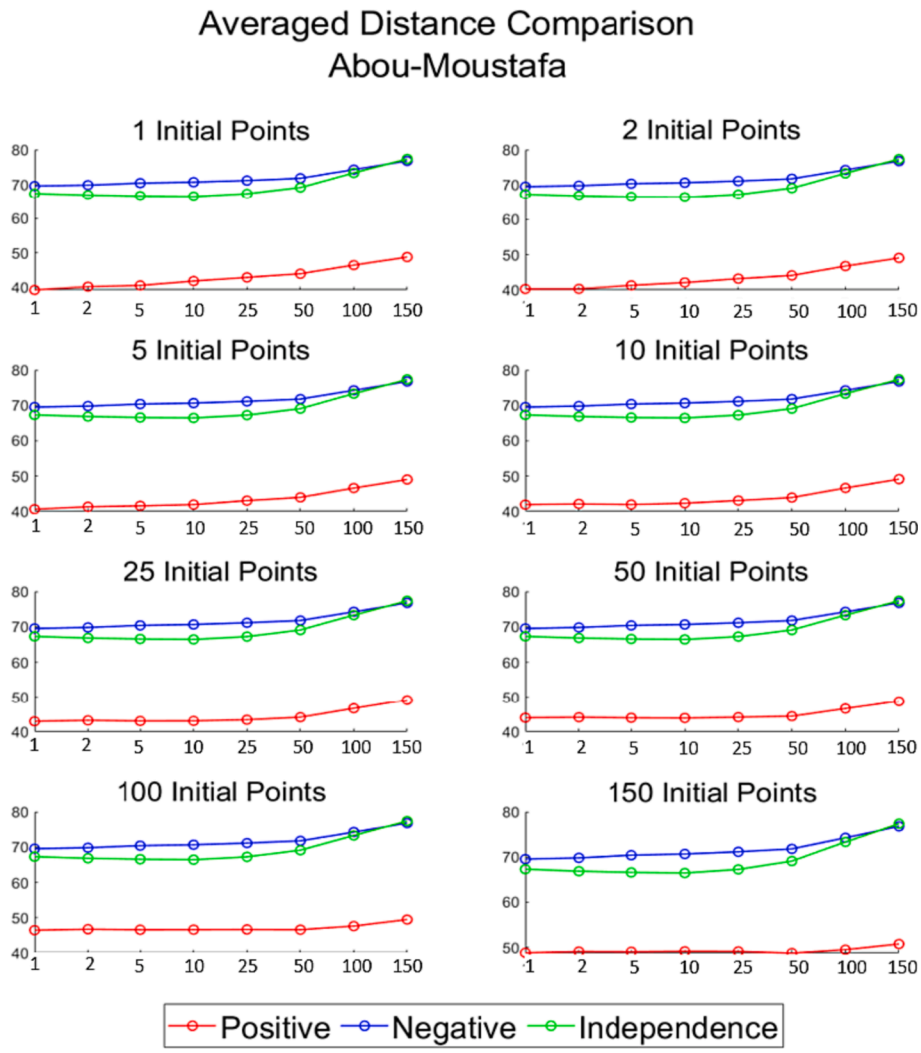

Fig. 12. Comparison of the average Abou-Moustafa distances between the positive Bayesian Networks and a) themselves (red), b) the negative cases (blue), and c) the independence case (green), classified by the number of initial points. (For interpretation of the references to color in this figure legend, the reader is referred to the web version of this article.)

or practically zero values in all the elements except the diagonals. Moreover, in the case of 1 initial point, it can be observed how high values of conditional rank correlation cause high correlation values in practically the whole correlation matrix, and these values decrease globally when the conditional rank correlation decreases. In the case of 150 initial points, it can be appreciated how the correlation affects the structure globally, but it is limited by the number of initial points. In other words, despite setting high correlation values, the most distant elements present low correlation values. Therefore, it can be concluded that the number of initial points presents a limiting effect on the correlation when high conditional rank values are used in constructing the Bayesian network. This aspect must be considered in the parameter setting process of the Bayesian network since an incorrect choice of the number of starting points may distort the result of the correlation matrix.

In order to conclude this section of the study, the distances among the Bayesian networks were calculated, aiming to quantify the differences originated by the conditional rank correlation and to compare them with the effect of the number of initial points. Accordingly, Table 3 presents the distances of the Bayesian networks using the Abou-Moustafa metric. The table shows that high values of conditional rank correlation provoke an increase in the distances similarly to the number of initial points. However, a slight difference in the conditional rank correlation provokes similar distance values to those obtained comparing two Bayesian networks with the same conditional rank correlation value and with 1 and 150 starting points, i.e., a slight difference in conditional rank correlation provokes a similar impact that a significant change in the number of initial points (from 1 to 150). For this reason, it can be concluded that conditional rank correlation values have a more severe effect on the correlation matrix due to their global behavior.

5.4. Results and discussion

After analyzing how the number of initial points and the conditional rank correlation affect the Bayesian network, the influence of these parameters on the generated variability is studied. For this purpose, 12 Bayesian networks with different conditional rank correlations (0.2, 0.6, 0.8) were created for the cases of 1 and 150 initial points and considering the bridge properties of steel members' thicknesses and Young's modulus.

A total of 500 samples were generated for each Bayesian network, assuming that the nodes follow a beta distribution with bounds of [-2, 2] mm for the thicknesses and [170,210] GPa for the Young's modulus. Each sample contains 879 thickness or Young's modulus values (one for each bridge element). In order to visualize the variability created, the

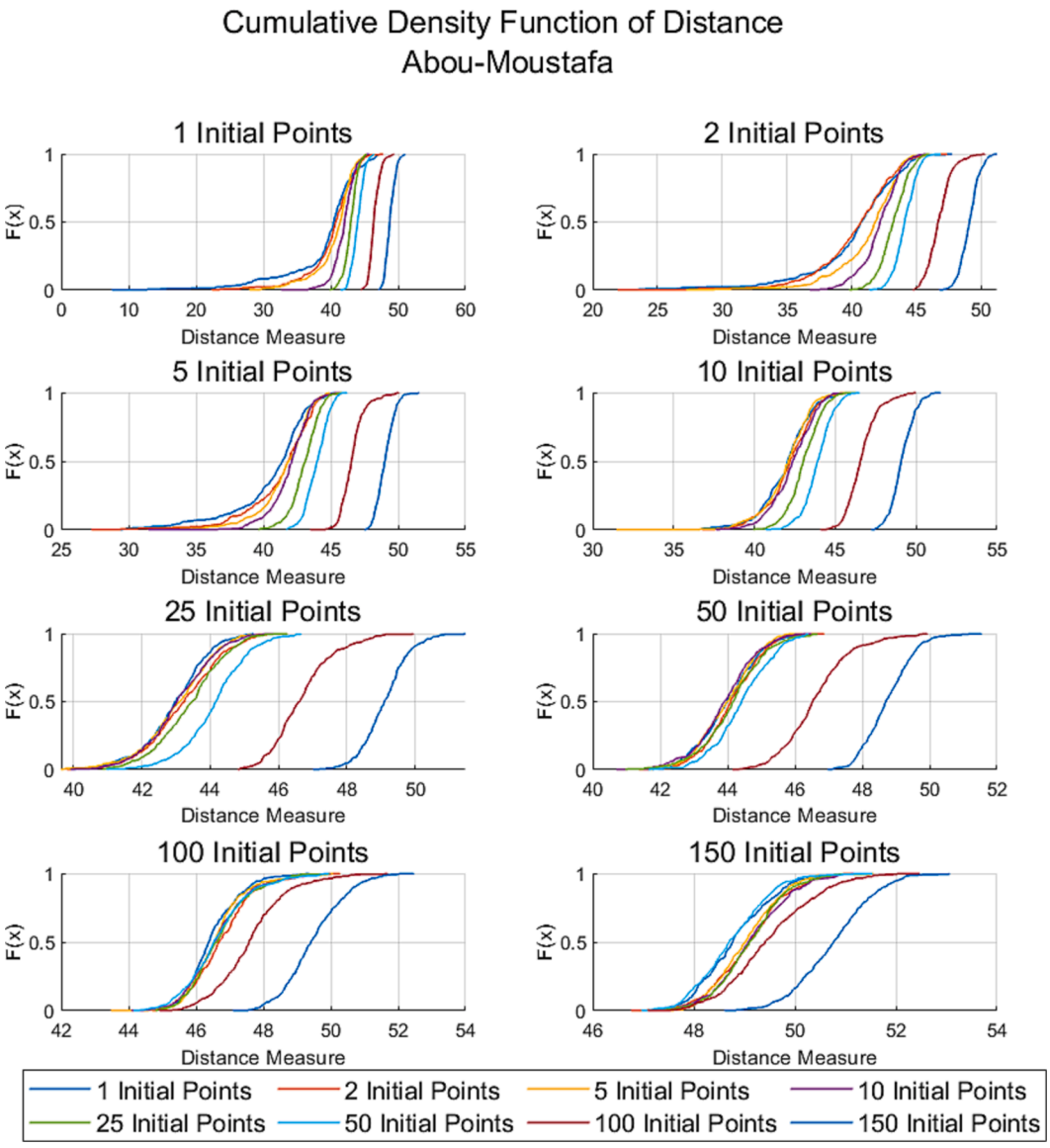

Fig. 13. Cumulative density functions of the Abou-Moustafa distances obtained among the sets of BNs classified as a function of the number of initial points.

Table 2
Mean and standard deviation of distance measures of 100 Bayesian networks for a different number of starting points using the Abou-Moustafa metric.

Initial Points	Averaged Distance	σ
1	39.191	5.901
2	40.649	3.181
5	41.608	2.000
10	42.242	1.403
25	43.320	1.066
50	44.427	0.930
100	47.425	0.980
150	50.785	0.815

cumulative density function for each of the 500 samples was plotted. Fig. 16 shows the thickness variability for the six generated Bayesian networks.

As can be observed, low correlation values induce a relatively uniform distribution of the bridge properties in their variation range. For this reason, the 500 simulated samples present very similar results. With high conditional rank correlation values, the bridge properties tend to become more homogeneous and agglutinated within the variation range, with less variability per sample. This entails the creation of more different samples for the same Bayesian network. In addition, in the cases of higher correlation values, more different samples can be seen in the case of 1 initial point concerning the case of 150 initial points. This fact is due to the limiting effect of the number of initial points on the Bayesian network correlation, as mentioned in the previous section.

Finally, an algorithm has been developed to visualize the generated variability in the bridge that automatically establishes a color scale in the FE model based on each element value. Fig. 17 shows the thickness variability of one of the 500 samples for 1 initial point and correlations of 0.2, 0.6, and 0.8. This figure shows how the increase of the conditional rank correlation generates more similar values in the closest elements of the bridge. For low conditional rank correlation values, the bridge properties are practically random, and almost no relationship between nearby elements can be observed.

Moreover, the effect of the different parameters of the Bayesian network on the output (dynamic) responses of the FE model was analyzed. For this purpose, a total of 6000 simulations were performed with different values of conditional rank correlation (0.2, 0.6, 0.8) for the cases of 1 and 150 initial points. The 12 Bayesian networks of the previous section were employed to generate the variability of the FE

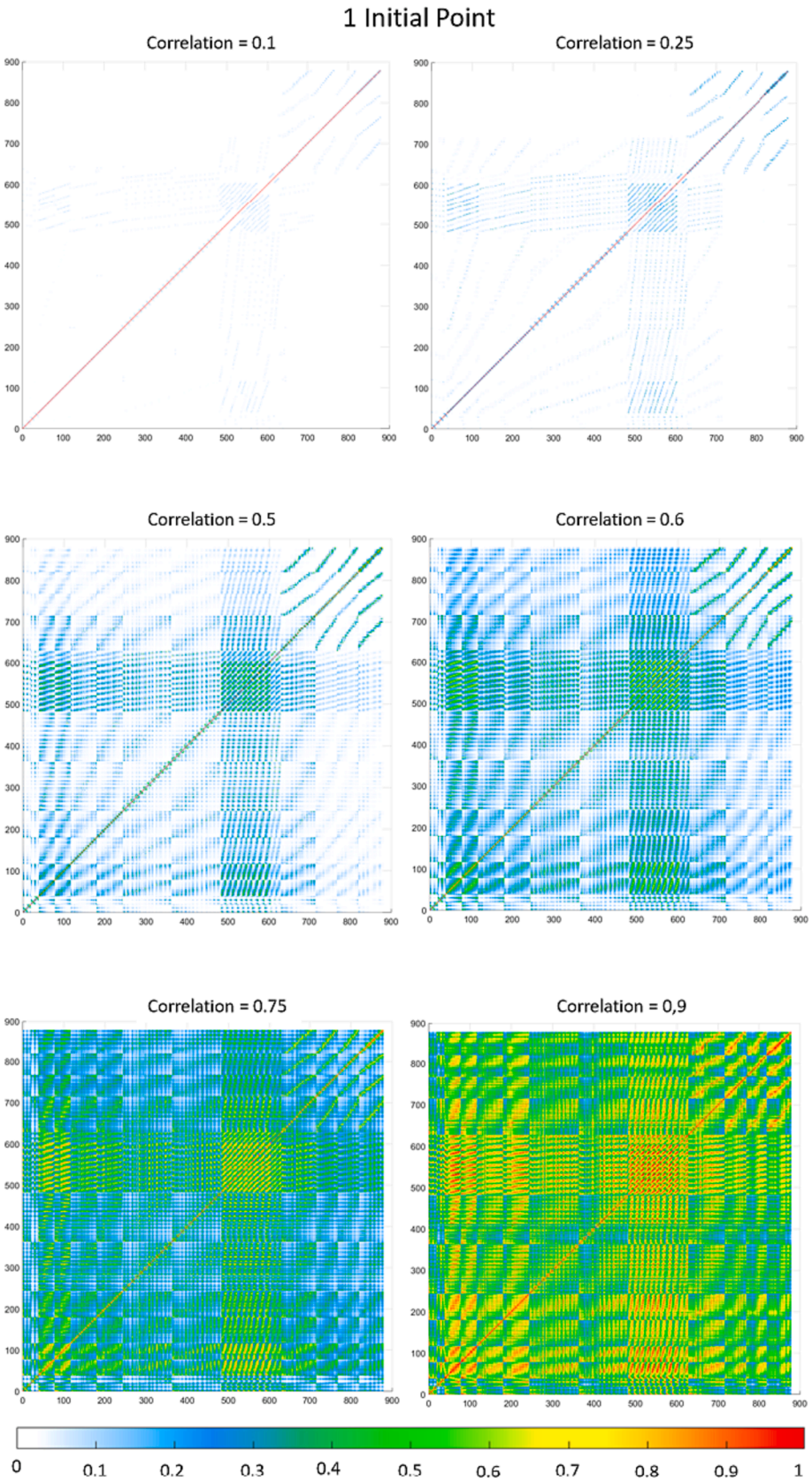

Fig. 14. Comparison of the correlation matrices obtained for 1 initial point and multiple conditional rank correlation values.

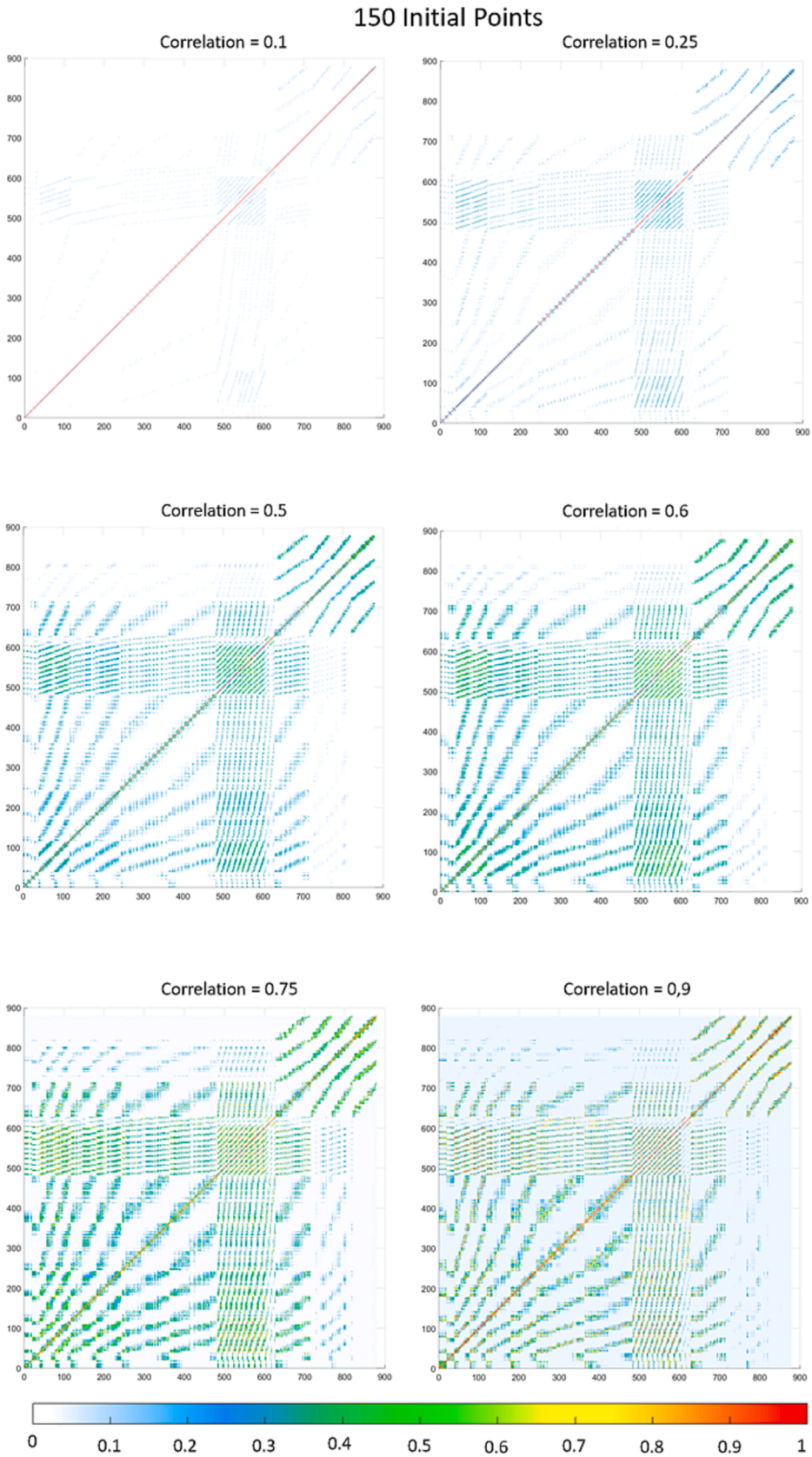

Fig. 15. Comparison of the correlation matrices obtained for 150 initial points and multiple conditional rank correlation values.

Table 3
Abou-Moustafa distances obtained among 12 Bayesian networks with different conditional rank correlation values and number of initial points.

Abou-Moustafa													
Correlation		1 Initial Point						150 Initial Point					
		Correlation											
		0.1	0.25	0.5	0.6	0.75	0.9	0.1	0.25	0.5	0.6	0.75	0.9
1 Initial Point	0.1	0.0	9.1	28.1	39.3	64.8	109.1	3.8	12.0	34.3	47.7	76.2	173.0
	0.3	9.1	0.0	20.3	32.2	58.8	104.0	10.1	9.1	28.9	42.3	71.2	169.1
	0.5	28.1	20.3	0.0	12.8	41.2	88.1	28.4	22.5	22.9	32.6	59.2	159.3
	0.6	39.3	32.2	12.8	0.0	29.7	77.7	39.5	33.5	26.6	31.4	53.8	154.1
	0.8	64.8	58.8	41.2	29.7	0.0	53.5	64.8	59.0	46.2	42.8	50.5	143.8
	0.9	109.1	104.0	88.1	77.7	53.5	0.0	108.9	103.5	88.0	79.9	69.2	131.4
150 Initial Point	0.1	3.8	10.1	28.4	39.5	64.8	108.9	0.0	10.1	33.2	46.7	75.5	173.5
	0.3	12.0	9.1	22.5	33.5	59.0	103.5	10.1	0.0	24.3	38.5	68.3	169.5
	0.5	34.3	28.9	22.9	26.6	46.2	88.0	33.2	24.3	0.0	15.2	47.7	156.2
	0.6	47.7	42.3	32.6	31.4	42.8	79.9	46.7	38.5	15.2	0.0	34.5	148.0
	0.8	76.2	71.2	59.2	53.8	50.5	69.2	75.5	68.3	47.7	34.5	0.0	129.9
	0.9	173.0	169.1	159.3	154.1	143.8	131.4	173.5	169.5	156.2	148.0	129.9	0.0

model properties. The frequencies of the first five vibration modes were extracted as output responses of the FE model. The histograms of the first natural frequency with the different configurations of initial points and conditional rank correlation values are presented in Fig. 18.

These figures show how high values of conditional rank correlation cause wider histograms and more extreme frequency values than in the simulations with lower conditional rank correlation values. This is because high conditional rank correlation values provoke more homogeneous values for each simulation, so the properties of the FE model behave more globally and acquire less dissimilar values. Regarding the initial points, the results are similar for the same value of conditional rank correlation, as shown in Fig. 19, where the cumulative density function (CDF) of the first natural frequency of each configuration of the Bayesian network is plotted. This figure shows how the CDFs are almost identical for the same conditional rank correlation values independently of the number of initial points. Besides, increasing the conditional rank correlation generates more extreme values in the dynamic responses, thus confirming the previous observations in the histograms. In addition, it can be highlighted that some vibration modes are more susceptible than others to the generated variability with the same Bayesian network configuration. This is because not all modes present the same sensitivity to the thickness variables and Young's modulus. This difference in sensitivity causes the variation bounds of the dynamic responses to be considerably wider in some modes.

As could be observed, the initial points and the conditional rank correlation have a strong influence on the generated variability and on the dynamic responses of the model. The characterization of these parameters could follow two approaches, i) based on experimental data or ii) computational using dynamic or static data as reference and applying a calibration framework. Following the first approach, the initial points could be the structural elements for which in situ measurements are available and the values of the child nodes are computed using inference. For conditional rank correlation, this approach would be more complex, as it would require a large number of measurements to obtain a robust value. The second approach would be to computationally estimate the initial points and conditional rank correlation in calibration frameworks. The disadvantage of this second approach is that it can lead to convergence problems in the optimization process. For this reason, an appropriate approach may involve determining the number of initial points experimentally and then computing the conditional rank correlation values within the optimization framework. However, the parameterization of the conditional rank correlation can be performed using multiple approaches such as different correlation values according to the profile type, the connection type, or its degree of exposure to environmental conditions. This requires an iterative framework of parameterization, sensitivity analysis and calibration. In addition, due to the nature of the proposed methodology, a new framework for sensitivity analysis and calibration must be developed. However, all

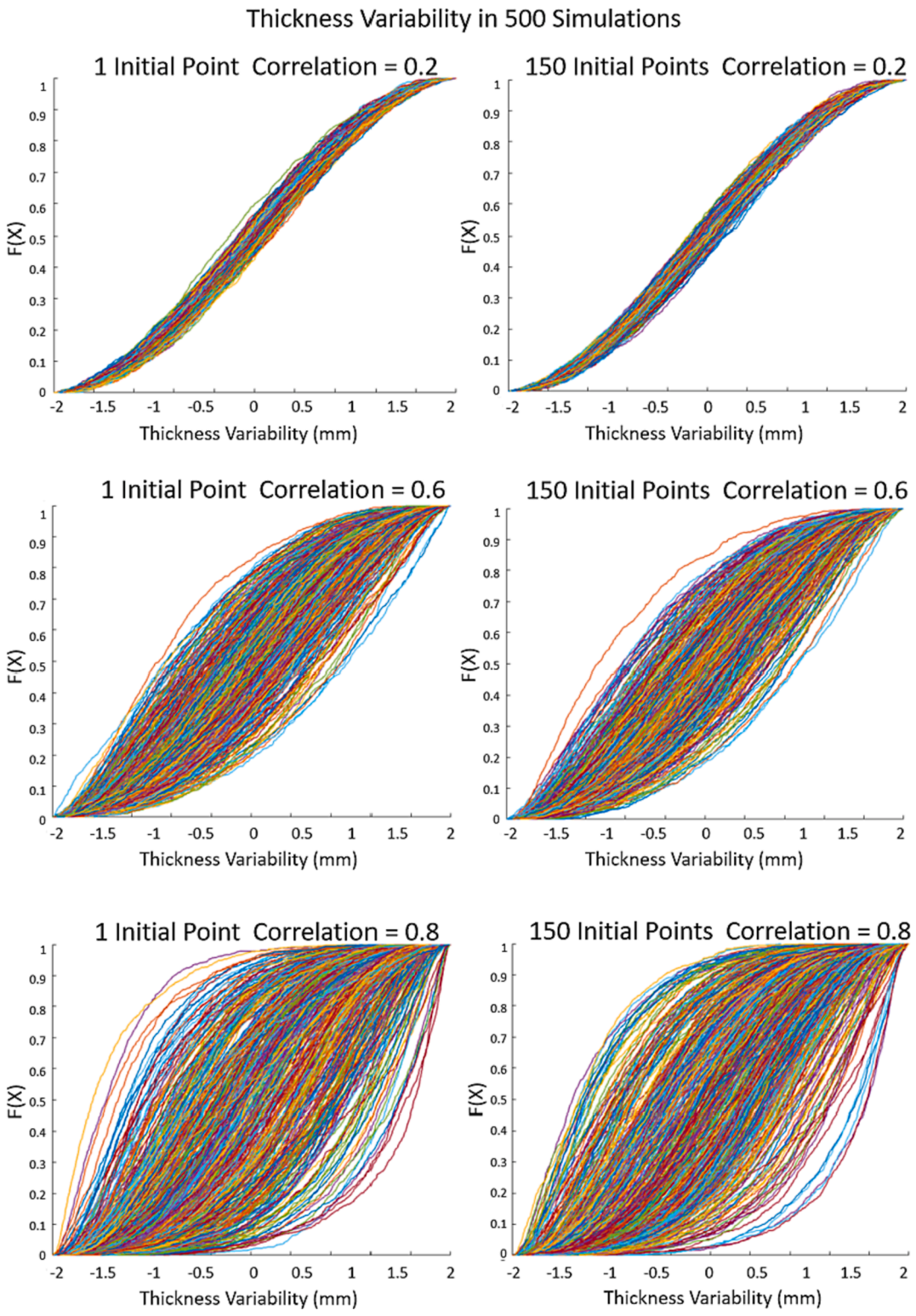

Fig. 16. Cumulative density function of steel members' thicknesses for 500 simulations with different configurations of initial points and conditional rank correlation values.

these issues are beyond the scope of this paper and will be addressed in a future work.

Finally, the computational cost of the methodology was evaluated using three different computers. The first is a medium–high-range laptop model (DELL G5), the second is a custom computer designed for these types of simulations, and the third is a computing server. The features of the computers are summarized in Table 4. The computational cost was divided into two parts. First, the consuming time to run the developed algorithm (BN time). This entails the time the algorithm spent copying the FE model, creating the geometry and the material for each element, traversing the structure and assigning the parent-children relationships, and finally creating the DAG structure, the correlation matrix, and, thus, the Bayesian network. This algorithm part is only simulated once for each Bayesian network configuration. Secondly, the computational cost

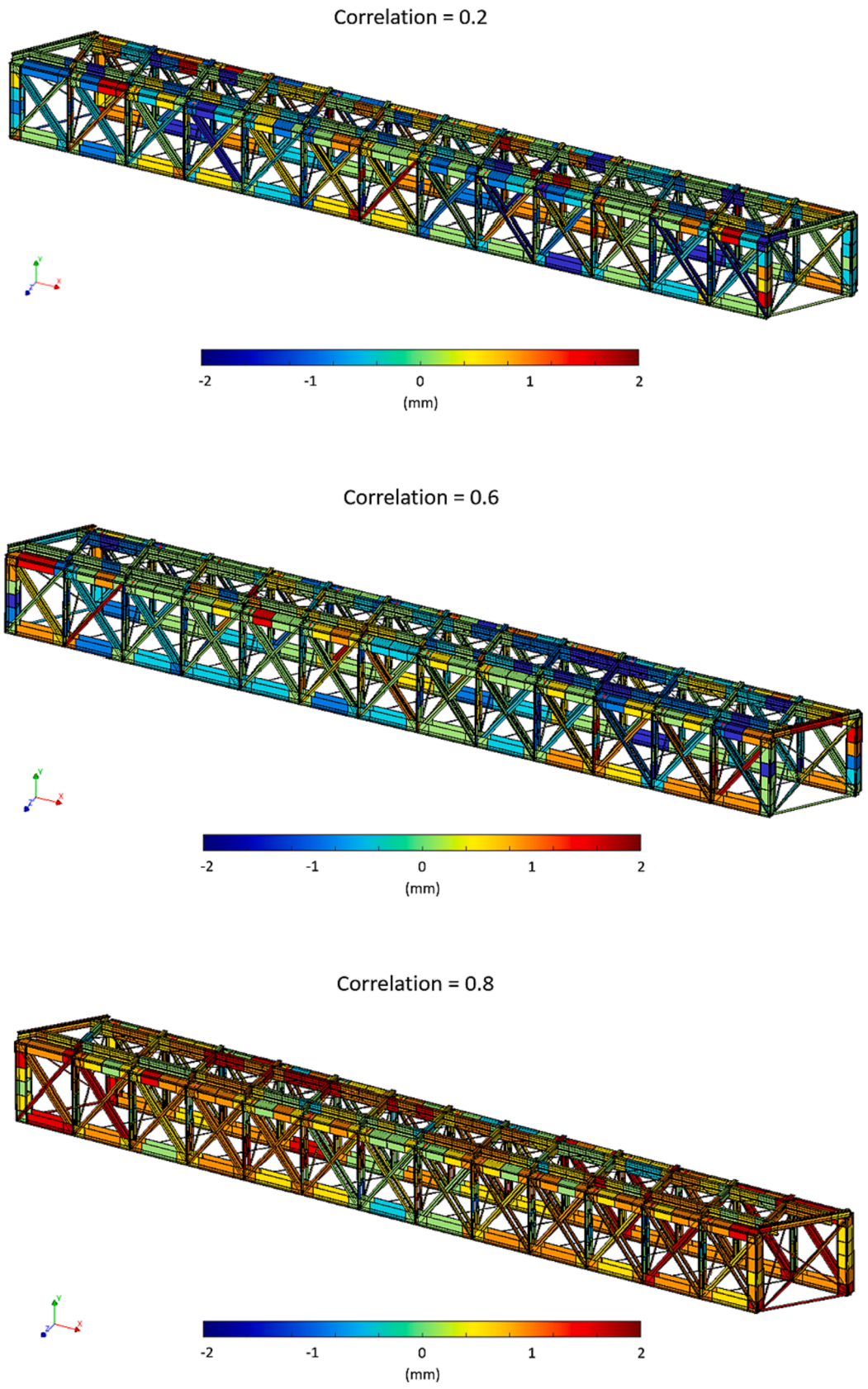

Fig. 17. Graphical representation of thickness variability with different conditional rank correlation values.

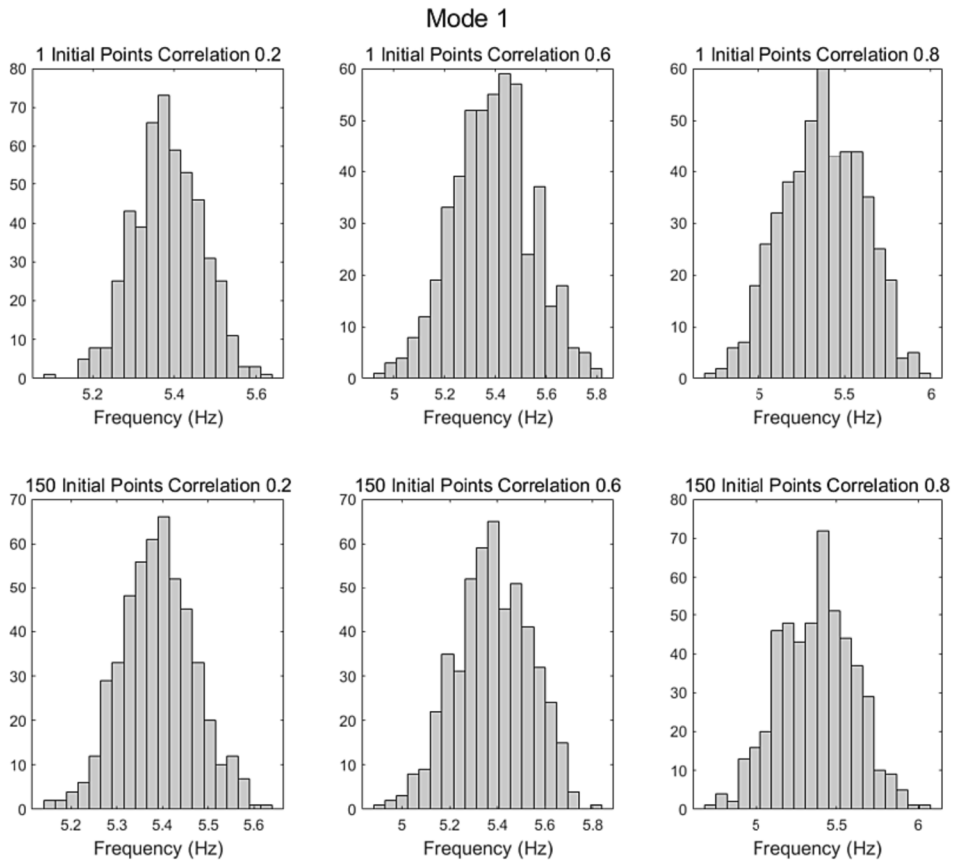

Fig. 18. Histograms of the first natural frequency for 500 simulations with different configurations of initial points and conditional rank correlation values.

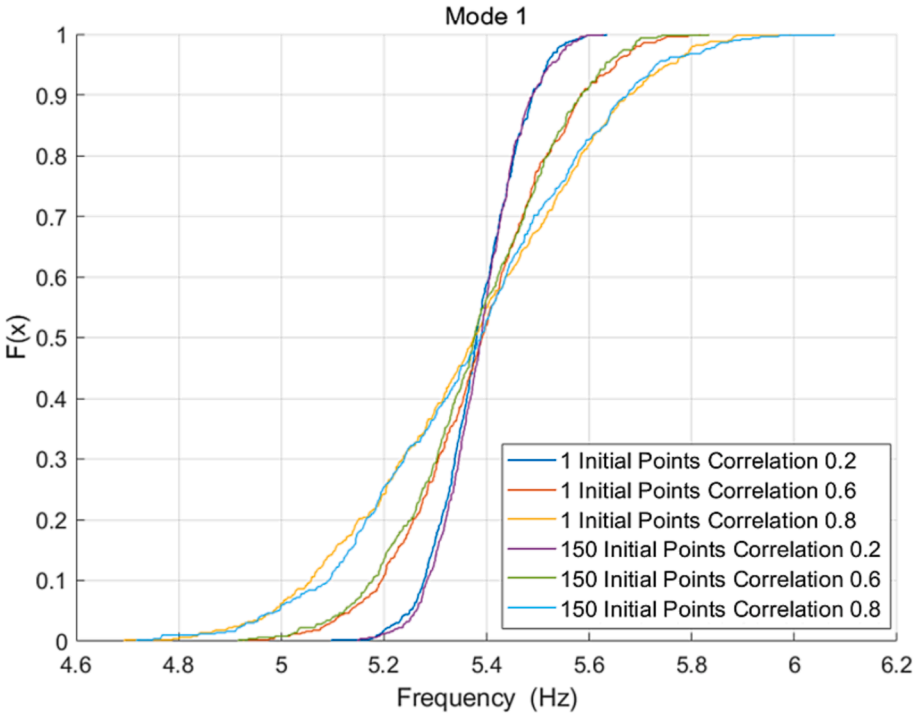

Fig. 19. Cumulative density function of the first natural frequency for 500 simulations with different configurations of initial points and conditional rank correlation values.

Table 4
Features of the three computers employed to quantify the computational cost.

	Features				
	Model	Reading/Writing SSD speed (Mb/s)	CPU model	Cores	Base/ Max Frequency (GHz)
PC1	Dell G5	3500 /2300	Intel i7 9750H	12	2.6/4.5
PC2	Custom	2200 /1900	AMD Ryzen 9 3950X	16	3.5/4.7
PC3	Server	7500/6850	2 X AMD EPYC 7513	2 X 32	2.6/3.65

Table 5
Computational cost of the BN creation and simulation of 100 samples for the three employed computers.

	Model	BN time (min)	100 Simulations time (min)	Total time (s)
PC1	Dell G5	12.85	24.36	14.61
PC2	Custom	7.03	10.18	6.11
PC3	Server	17.90	5.73	3.44

of simulating 100 samples with different thicknesses and Young's modulus values for each element was evaluated. Table 5 summarizes the computational cost of the two algorithm steps for the three computers.

As observed, the time to build both Bayesian networks (BN time) range from 7.03 to 17.9 min, depending on the computer employed. In this step, the CPU speed is crucial since it is characterized by performing most calculations in series. Thus, it is recommended to use computers with higher CPU speed (such as PC2) to carry out this part of the process since the number of cores is not a determining factor. Regarding the simulation time for 100 simulations, it varies from 5.73 to 24.36 min, which translates into a speed of 3.44 to 14.61 s per simulation. As this part of the code is parallelized, the number of cores is crucial and more important than the CPU speed. This can be seen in the results where the highest simulation speed was obtained for the computer with more cores (PC3) which obtained a speed of 3.44 s per simulation. In this regard, it should be highlighted that if the employed computer does not have a sufficiently powerful hard disk, it can act as a bottleneck due to the read/write workload required by the FE model simulations, so despite increasing the number of cores, the simulation speed will not increase.

6. Conclusions

This paper proposes using Gaussian Copula-based Bayesian Network (GCBN) for spatial variability characterization in aging steel bridges. This work involved the development of the methodology and the assessment of the generated variability. As future work, the practical implementation to model the corrosion variability in a real case study could be performed. For this purpose, a methodology should be defined for the optimization of the parameters of the Bayesian network to ensure that the generated models are representative of the real structure. In this paper a methodology was developed that automatically creates a Bayesian network and induces the generated variability in the FE model. As a simplification to carry out the study of the variability generated, only positive and uniform values of conditional rank correlation were assumed for each pair of nodes of the BN. Thus, the conditional rank correlation variable is defined as the correlation between any pair of adjacent structural elements. The main findings of the study are summarized in the following:

- From the study of the controllable parameters of the automatic generation process of the Bayesian Network, it can be concluded that the conditional rank correlation globally affects the correlation matrix that defines the Bayesian network, while the initial points mainly affect the correlation of the most distant elements in the structure. Besides, a high number of initial points limits the effect that the conditional rank correlation exerts on the correlation matrix. This fact implies that the correlation matrix maintains low values in the more distant elements despite the employment of high conditional rank correlation values. Regarding the influence of the controllable parameters in the FE model, it can be noted that higher conditional rank correlation values create samples with more homogeneous properties in the bridge. Therefore, more extreme values in the dynamic responses are obtained. The initial points produce a lighter effect than the conditional rank correlation on the generated variability and, therefore, on the dynamic responses.
- About the methodology, it is highlighted that the GCBN is a highly efficient tool for modeling complex dependencies, thus overcoming the drawbacks presented in classical random fields. Moreover, it has a low computational cost thanks to the Gaussian copulas and the efficiency of the automatic generation algorithms, making it ideal for high-dimensional problems such as the one presented in this study. Nonetheless, due to the high complexity of modeling the corrosion phenomena and the typical lack of experimental measurements, it is recommended to select the parameter settings of the Bayesian network (initial points and conditional rank correlation) based on collected data of the bridge properties such as the static or dynamic responses.
- Overall, it can be concluded that the synergies produced between the developed algorithm, which provide a fully automatic generation of the Bayesian network, and the use of the GCBN allow us to accurately model, at a low computational cost, the properties variability in high-dimensional problems of complex structures, such as aging steel bridges, making the methodology a robust process for the generation of highly detailed probabilistic FE models. For other bridge typologies, such as masonry or concrete bridges, the use of the Bayesian network can also be a very effective approach. In micro-modeling approaches it can define the dependencies between the units, the mortar joints and their interfaces in a more robust way. In addition, the use of experimental data together the use of inference can be an accurate approach to model the damage in the structure. Notice that performing inference using traditional models such as random fields would not be a straightforward task as it is with BNs.
- Finally, some lines of action are underlined to improve the methodology in further work regarding different aspects, such as increasing the discretization level of the structure, further enhancing the modeling flexibility of the Bayesian network by implementing constraints that choose different values of conditional rank correlation depending on the element type and connection or improving the representation of the properties variability by applying Bayesian inference on the network if experimental data of the structure were available.

CRediT authorship contribution statement

B. Barros: Methodology, Software, Investigation. **B. Conde:** Conceptualization, Investigation, Supervision, Writing – review & editing. **B. Riveiro:** Funding acquisition, Supervision, Writing – review & editing. **O. Morales-Nápoles:** Methodology, Software, Resources, Investigation, Supervision, Writing – review & editing.

Declaration of Competing Interest

The authors declare that they have no known competing financial interests or personal relationships that could have appeared to influence the work reported in this paper.

Data availability

The authors do not have permission to share data.

Acknowledgments

This project has received funding from the European Union's Horizon 2020 research and innovation program under grant agreement No. 958171. This work has been partially supported by the Spanish Ministry of Science and Innovation through the PONT3 project Ref. PID2021-124236OB-C33. This work has also been supported by the Spanish Ministry of Science, Innovation, and Universities through the grant PRE2019-087331 for the training of predoctoral researchers. This document reflects only the views of the authors. Neither the Innovation and Networks Executive Agency (INEA) nor the European Commission is in any way responsible for any use that may be made of the information it contains.

References

[1] P. Icke and C. Margheriti, "The benefits and use of FE modelling in bridge assessment and design," in *Proceedings of the Sixth International Conference on Bridge Maintenance, Safety and Management*, no. Hendy, 2012, pp. 3191–3197.
[2] Bouzas O, Conde B, Cabaleiro M, Riveiro B. A holistic methodology for the non-destructive experimental characterization and reliability-based structural assessment of historical steel bridges. Eng Struct 2022;vol. 270, no. May:114867. https://doi.org/10.1016/j.engstruct.2022.114867.
[3] Conde B, Ramos LF, Oliveira DV, Riveiro B, Solla M. Structural assessment of masonry arch bridges by combination of non-destructive testing techniques and three-dimensional numerical modelling: Application to Vilanova bridge. Eng Struct 2017;148:621–38. https://doi.org/10.1016/j.engstruct.2017.07.011.
[4] Sánchez-Aparicio LJ, Bautista-De Castro Á, Conde B, Carrasco P, Ramos LF. Non-destructive means and methods for structural diagnosis of masonry arch bridges. Autom Constr 2019;104(May):360–82. https://doi.org/10.1016/j.autcon.2019.04.021.
[5] Armstrong CG. Modelling requirements for finite-element analysis. Comput Des 1994;26(7):573–8. https://doi.org/10.1016/0010-4485(94)90088-4.
[6] Appuhamy JMRS, Kaita T, Ohga M, Fujii K. Prediction of residual strength of corroded tensile steel plates. Int J Steel Struct 2011;11(1):65–79. https://doi.org/10.1007/S13296-011-1006-6.
[7] S. López, N. Makoond, A. Sánchez-Rodríguez, J. M. Adam, and B. Riveiro, "Learning from failure propagation in steel truss bridges," vol. 152, no. May, 2023, doi: 10.1016/j.engfailanal.2023.107488.
[8] J. R. Kayser and A. S. Nowak, "Capacity Loss Due to Corrosion in Steel-Girder Bridges," *J. Struct. Eng.*, 1989, [Online]. Available: https://doi.org/10.1061/(ASCE)0733-9445(1989)115:6(1525).
[9] Garbatov Y, Guedes Soares C, Parunov J, Kodvanj J. Tensile strength assessment of corroded small scale specimens. Corros Sci 2014;85:296–303. https://doi.org/10.1016/j.corsci.2014.04.031.
[10] Wang Y, Xu S, Li A. Flexural performance evaluation of corroded steel beams based on 3D corrosion morphology. Struct Infrastruct Eng 2020;16(11):1562–77. https://doi.org/10.1080/15732479.2020.1713169.
[11] Wang Y, Xu S, Wang H, Li A. Predicting the residual strength and deformability of corroded steel plate based on the corrosion morphology. Constr Build Mater 2017;152:777–93. https://doi.org/10.1016/j.conbuildmat.2017.07.035.
[12] Conde B, Eguía P, Stavroulakis GE, Granada E. Parameter identification for damaged condition investigation on masonry arch bridges using a Bayesian approach. Eng Struct 2018;172(June):275–84. https://doi.org/10.1016/j.engstruct.2018.06.040.
[13] Barros B, Conde B, Sánchez-Aparicio LJ, Cabaleiro M, Bouzas O, Riveiro B. "Model Calibration of a Historic Masonry Arch Bridge Using a Probabilistic Approach", Lecture Notes. Civ Eng 2022;vol. 200 LNCE:75–83. https://doi.org/10.1007/978-3-030-91877-4_9.
[14] Liu Y, Li J, Sun S, Yu B. Advances in Gaussian random field generation: a review. Comput Geosci 2019;23(5):1011–47. https://doi.org/10.1007/s10596-019-09867-y.
[15] Chen NZ, Guedes Soares C. Spectral stochastic finite element analysis for laminated composite plates. Comput Methods Appl Mech Eng 2008;197(51–52):4830–9. https://doi.org/10.1016/j.cma.2008.07.003.
[16] Noh HC, Park T. Response variability of laminate composite plates due to spatially random material parameter. Comput Methods Appl Mech Eng 2011;200(29–32):2397–406. https://doi.org/10.1016/j.cma.2011.03.020.
[17] Zhang JZ, Huang HW, Zhang DM, Zhou ML, Tang C, Liu DJ. Effect of ground surface surcharge on deformational performance of tunnel in spatially variable soil. Comput Geotech 2021;vol. 136, no. April:104229. https://doi.org/10.1016/j.compgeo.2021.104229.
[18] C. M. P. Hart, O. Morales-Nápoles, and S. N. Jonkman, "Influence of spatial variation of foundation in the design of shear-keys in immersed tunnel structures," *submmited Publ.*
[19] Dilip DM, Sivakumar Babu GL. Influence of Spatial Variability on Pavement Responses Using Latin Hypercube Sampling on Two-Dimensional Random Fields. J Mater Civ Eng 2014;26(11):1–7. https://doi.org/10.1061/(asce)mt.1943-5533.0000994.
[20] Eliáš J, Vorechovský M, Le J. Lattice Modeling of Concrete Fracture Including Material Spatial Randomness. Eng Mech 2013;20(5):413–26.
[21] Eliáš J, Vořechovský M, Skoček J, Bažant ZP. Stochastic discrete meso-scale simulations of concrete fracture: Comparison to experimental data. Eng Fract Mech 2015;135:1–16. https://doi.org/10.1016/j.engfracmech.2015.01.004.
[22] P. Ni, J. Li, H. Hao, and H. Zhou, "Reliability based design optimization of bridges considering bridge-vehicle interaction by Kriging surrogate model," *Eng. Struct.*, vol. 246, no. October 2020, p. 112989, 2021, doi: 10.1016/j.engstruct.2021.112989.
[23] Shafei B, Alipour A. Application of large-scale non-Gaussian stochastic fields for the study of corrosion-induced structural deterioration. Eng Struct 2015;88:262–76. https://doi.org/10.1016/j.engstruct.2014.12.024.
[24] Papakonstantinou KG, Shinozuka M. Probabilistic model for steel corrosion in reinforced concrete structures of large dimensions considering crack effects. Eng Struct 2013;57:306–26. https://doi.org/10.1016/j.engstruct.2013.06.038.
[25] D. C. Feng, S. C. Xie, Y. Li, and L. Jin, "Time-dependent reliability-based redundancy assessment of deteriorated RC structures against progressive collapse considering corrosion effect," *Struct. Saf.*, vol. 89, no. November 2020, p. 102061, 2021, doi: 10.1016/j.strusafe.2020.102061.
[26] Beckmann C, Hohe J. Effects of material uncertainty in the structural response of metal foam core sandwich beams. Compos Struct 2014;113(1):382–95. https://doi.org/10.1016/j.compstruct.2014.03.030.
[27] Casciati S, Domaneschi M. Random imperfection fields to model the size effect in laboratory wood specimens. Struct Saf 2007;29(4):308–21. https://doi.org/10.1016/j.strusafe.2006.07.014.
[28] Moshtaghin AF, Franke S, Keller T, Vassilopoulos AP. Random field-based modeling of size effect on the longitudinal tensile strength of clear timber. Struct Saf 2016;58:60–8. https://doi.org/10.1016/j.strusafe.2015.09.002.
[29] Shojai S, Schaumann P, Brömer T. Probabilistic modelling of pitting corrosion and its impact on stress concentrations in steel structures in the offshore wind energy. Mar Struct 2022;84(April). https://doi.org/10.1016/j.marstruc.2022.103232.
[30] Woloszyk K, Garbatov Y. Random field modelling of mechanical behaviour of corroded thin steel plate specimens. Eng Struct 2022;212(May):2020. https://doi.org/10.1016/j.engstruct.2020.110544.
[31] Woloszyk K, Garbatov Y. An enhanced method in predicting tensile behaviour of corroded thick steel plate specimens by using random field approach. Ocean Eng 2020;vol. 213, no. July:107803. https://doi.org/10.1016/j.oceaneng.2020.107803.
[32] Xiang W, Zhou W. A non-parametric Bayesian network model for predicting corrosion depth on buried pipelines. Corrosion 2020;76(3):235–47. https://doi.org/10.5006/3421.
[33] Morato PG, Papakonstantinou KG, Andriotis CP, Nielsen JS, Rigo P. Optimal inspection and maintenance planning for deteriorating structural components through dynamic Bayesian networks and Markov decision processes. 2021, p. 102140 Struct Saf 2022;94(October). https://doi.org/10.1016/j.strusafe.2021.102140.
[34] Ahmed M, Moselhi O, Bhowmick A. Two-tier data fusion method for bridge condition assessment. Can J Civ Eng 2018;45(3):197–214. https://doi.org/10.1139/cjce-2017-0160.
[35] Guo H, Dong Y. Dynamic Bayesian network for durability of reinforced concrete structures in long-term environmental exposures. Eng Fail Anal 2022;vol. 142, no. July:106821. https://doi.org/10.1016/j.engfailanal.2022.106821.
[36] A. Maroni, E. Tubaldi, D. V. Val, H. McDonald, and D. Zonta, "Using Bayesian networks for the assessment of underwater scour for road and railway bridges," *Struct. Heal. Monit.*, pp. 1–15, 2020, doi: 10.1177/1475921720956579.
[37] Luque J, Straub D. Reliability analysis and updating of deteriorating systems with dynamic Bayesian networks. Struct Saf 2016;62:34–46. https://doi.org/10.1016/j.strusafe.2016.03.004.
[38] Hackl J, Kohler J. Reliability assessment of deteriorating reinforced concrete structures by representing the coupled effect of corrosion initiation and progression by Bayesian networks. Struct Saf 2016;62:12–23. https://doi.org/10.1016/j.strusafe.2016.05.005.
[39] Gehl P, D'Ayala D. Development of Bayesian Networks for the multi-hazard fragility assessment of bridge systems. Struct Saf 2016;60:37–46. https://doi.org/10.1016/j.strusafe.2016.01.006.
[40] Luque J, Straub D. Risk-based optimal inspection strategies for structural systems using dynamic Bayesian networks. 2018, pp. 68–80 Struct Saf 2019;76(August). https://doi.org/10.1016/j.strusafe.2018.08.002.
[41] Ma Y, Wang L, Zhang J, Xiang Y, Liu Y. Bridge Remaining Strength Prediction Integrated with Bayesian Network and In Situ Load Testing. J Bridg Eng 2014;19(10):1–11. https://doi.org/10.1061/(asce)be.1943-5592.0000611.
[42] Zhu J, Zhang W, Li X. Fatigue damage assessment of orthotropic steel deck using dynamic Bayesian networks. 2018, pp. 44–53 Int J Fatigue 2019;118(March). https://doi.org/10.1016/j.ijfatigue.2018.08.037.
[43] Y. Xu, B. Zhu, Z. Zhang, and J. Chen, "Hierarchical Dynamic Bayesian Network-Based Fatigue Crack Propagation Modeling Considering Initial Defects," *Sensors*, vol. 22, no. 18, 2022, doi: 10.3390/s22186777.
[44] R. Wang, L. Ma, C. Yan, and J. Mathew, "Structural reliability prediction of a steel bridge element using dynamic object oriented Bayesian network (DOOBN)," *ICQR2MSE 2011 - Proc. 2011 Int. Conf. Qual. Reliab. Risk, Maintenance, Saf. Eng.*, pp. 7–12, 2011, doi: 10.1109/ICQR2MSE.2011.5976559.
[45] Weber P, Medina-Oliva G, Simon C, Iung B. Overview on Bayesian networks applications for dependability, risk analysis and maintenance areas. Eng Appl Artif Intell 2012;25(4):671–82. https://doi.org/10.1016/j.engappai.2010.06.002.
[46] Marcot BG, Penman TD. Advances in Bayesian network modelling: Integration of modelling technologies. 2018, pp. 386–393 Environ Model Softw 2019;111(March). https://doi.org/10.1016/j.envsoft.2018.09.016.

[47] Hanea A, Morales Napoles O, Ababei D. Non-parametric Bayesian networks: Improving theory and reviewing applications. Reliab Eng Syst Saf 2015;144: 265–84. https://doi.org/10.1016/j.ress.2015.07.027.

[48] Paprotny D, Morales-Nápoles O, Worm DTH, Ragno E. BANSHEE–A MATLAB toolbox for Non-Parametric Bayesian Networks. SoftwareX 2020;12:100588. https://doi.org/10.1016/j.softx.2020.100588.

[49] Koot P, Mendoza-Lugo MA, Paprotny D, Morales-Nápoles O, Ragno E, Worm DTH. PyBanshee version (1.0): A Python implementation of the MATLAB toolbox BANSHEE for Non-Parametric Bayesian Networks with updated features. SoftwareX 2023;21:101279. https://doi.org/10.1016/j.softx.2022.101279.

[50] Morales-Nápoles O, Rajabi-Bahaabadi M, Torres-Alves GA, 't Hart CMP. Chimera: An atlas of regular vines on up to 8 nodes. Sci Data 2023;10(1):2–11. https://doi.org/10.1038/s41597-023-02252-6.

[51] Sebastian A, Dupuits EJC, Morales-Nápoles O. Applying a Bayesian network based on Gaussian copulas to model the hydraulic boundary conditions for hurricane flood risk analysis in a coastal watershed. Coast Eng 2017;125(March):42–50. https://doi.org/10.1016/j.coastaleng.2017.03.008.

[52] Torres-Alves GA, Morales-Nápoles O. Reliability analysis of flood defenses: The case of the Nezahualcoyotl dike in the aztec city of Tenochtitlan. Reliab Eng Syst Saf 2020;vol. 203, no. June:107057. https://doi.org/10.1016/j.ress.2020.107057.

[53] Ragno E, Hrachowitz M, Morales-Nápoles O. Applying non-parametric Bayesian networks to estimate maximum daily river discharge: potential and challenges. Hydrol Earth Syst Sci 2022;26(6):1695–711. https://doi.org/10.5194/hess-26-1695-2022.

[54] G. A. Torres-Alves, O. Morales-Nápoles, and S. N. Jonkman, "Bayesian Networks for estimating hydrodynamic forces on a submerged floating tunnel," *Proc. 31st Eur. Saf. Reliab. Conf. ESREL 2021*, pp. 2518–2524, 2021, doi: 10.3850/978-981-18-2016-8_292-cd.

[55] Thomas A, Kosgodagan A, Morales-Nápoles O, Maljaars J. Maintenance decision model for steel bridges: a case in the Netherlands. Struct Infrastruct Eng 2016. https://doi.org/10.1080/15732479.2016.1158194.

[56] Mendoza-Lugo MA, Delgado-Hernández DJ, Morales-Nápoles O. Reliability analysis of reinforced concrete vehicle bridges columns using non-parametric Bayesian networks. Eng Struct 2019;188(February):178–87. https://doi.org/10.1016/j.engstruct.2019.03.011.

[57] Morales-Nápoles O, Steenbergen RDJM. Large-Scale Hybrid Bayesian Network for Traffic Load Modeling from Weigh-in-Motion System Data. J Bridg Eng 2015;20(1): 1–10. https://doi.org/10.1061/(asce)be.1943-5592.0000636.

[58] Mendoza-Lugo MA, Morales-Nápoles O, Delgado-Hernández DJ. A Non-parametric Bayesian Network for multivariate probabilistic modelling of Weigh-in-Motion System Data. 2021, p. 100552 Transp Res Interdiscip Perspect 2022;13 (September). https://doi.org/10.1016/j.trip.2022.100552.

[59] J. Pearl, Probabilistic reasoning in intelligent systems: Networks of Plausible Inference. Los Angeles, 1988.

[60] Koski T, Noble JM. Bayesian Networks An introduction. John Wiley & Sons Ltd 2009.

[61] Ahmed SE. Bayesian Networks and Decision Graphs 2008;50(1):pp.

[62] Shachter RD, Kenley CR. Gaussian Influence Diagrams. Manage Sci 1989;35(5): 527–50. https://doi.org/10.1287/mnsc.35.5.527.

[63] Lauritzen SL. Propagation of probabilities, means, and variances in mixed graphical association models. J Am Stat Assoc 1992;87(420):1098–108. https://doi.org/10.1080/01621459.1992.10476265.

[64] Neil M, Tailor M, Marquez D. Inference in hybrid Bayesian networks using dynamic discretization. Stat Comput 2007;17(3):219–33. https://doi.org/10.1007/s11222-007-9018-y.

[65] Jordan MI, Ghahramani Z, Jaakkola TS, Saul LK. Introduction to variational methods for graphical models. Mach Learn 1999;37(2):183–233. https://doi.org/10.1023/A:1007665907178.

[66] Langseth H, Nielsen TD, Rumí R, Salmerón A. Mixtures of truncated basis functions. Int J Approx Reason 2012;53(2):212–27. https://doi.org/10.1016/j.ijar.2011.10.004.

[67] Langseth H, Nielsen TD, Rumí R, Salmerón A. Inference in hybrid Bayesian networks. Reliab Eng Syst Saf 2009;94(10):1499–509. https://doi.org/10.1016/j.ress.2009.02.027.

[68] Shaked M, Joe H. Multivariate Models and Dependence Concepts 1998;93(443):pp.

[69] R. B. Nelsen, An introduction to copulas. Portland, 2005.

[70] D. Kurowicka and R. . Cooke, "Distribution - Free Continuous Bayesian Belief Nets," 2003, doi: https://doi.org/10.1142/9789812703378_0022.

[71] A. M. Hanea, D. Kurowicka, and R. M. Cooke, "Hybrid Method for Quantifying and Analyzing Bayesian Belief Nets," 2006, doi: DOI: 10.1002/qre.808.

[72] Headrick TC. A Note on the Relationship between the Pearson Product-Moment and the Spearman Rank-Based Coefficients of Correlation. Open J Stat 2016;06 (06):1025–7. https://doi.org/10.4236/ojs.2016.66082.

[73] Church A, Yule GU, Kendall MG. An introduction to the theory of statistics. J Symb Log 1951;16(1):pp. https://doi.org/10.2307/2268667.

[74] Cooke RM. Experts in Uncertainty: Opinion and Subjective Probability in Science. New York: Oxford University Press; 1991.

[75] Morales O, Kurowicka D, Roelen A. Eliciting conditional and unconditional rank correlations from conditional probabilities. Reliab Eng Syst Saf 2008;93(5): 699–710. https://doi.org/10.1016/j.ress.2007.03.020.

[76] "Ansys SpaceClaim 3D CAD Modeling Software." [Online]. Available: https://www.ansys.com/products/3d-design/ansys-spaceclaim.

[77] Computational Mechanics department of TNO Building and construction research institute, "DIANA FEA BV Documentation." Delt,The Netherlands, 2003, [Online]. Available: https://dianafea.com.

[78] "MATLAB." The MathWorks Inc, Natick, Massachusetts:, [Online]. Available: https://es.mathworks.com/products/matlab.html.

[79] *AENOR Part 1: Corrosion of metals and alloys - Corrosivity of atmospheres - Classification, determination and estimation (ISO 92232012)*. .

[80] *AENOR Part 2: Corrosion of metals and alloys - Corrosivity of atmospheres - Guiding values for the corrosivity categories (ISO 9224:2012)*. .

[81] JCSS, "Probabilistic Model Code - Part 2: Load Models," pp. 1–73, 2001.

[82] M. Barbato, Q. Gu, and J. P. Conte, "Probabilistic Push-Over Analysis of Structural and Soil-Structure Systems," *J. Struct. Eng.*, no. November, pp. 1330–1341, 2010, doi: 10.1061/(ASCE)ST.1943-541X.0000231 CE.

[83] Park CB, Miller RD, Xia J. Multichannel analysis of surface waves. Geophysics 1999;64:800–8. https://doi.org/10.1190/1.1444590.

[84] AENOR, *Eurocode 3: Design of steel structures. Part 1-1: General rules and rules for buildings. UNE-EN 1993-1-1*. 2013.

[85] Morales-Nápoles O, Delgado-Hernández DJ, De-León-Escobedo D, Arteaga-Arcos JC. A continuous Bayesian network for earth dams' risk assessment: Methodology and quantification. Struct Infrastruct Eng 2014;10(5):589–603. https://doi.org/10.1080/15732479.2012.757789.

[86] O. Morales-Nápoles, A. M. Hanea, and D. T. H. Worm, "Experimental results about the assessments of conditional rank correlations by experts: Example with air pollution estimates," *Safety, Reliab. Risk Anal. Beyond Horiz. - Proc. Eur. Saf. Reliab. Conf. ESREL 2013*, no. 2009, pp. 1359–1366, 2014.

[87] Werner C, Bedford T, Cooke RM, Hanea AM, Morales-Nápoles O. Expert judgement for dependence in probabilistic modelling: A systematic literature review and future research directions. Eur J Oper Res 2017;258(3):801–19. https://doi.org/10.1016/j.ejor.2016.10.018.

[88] A. Kosgodagan, O. Morales-Nápoles, J. Maljaars, and W. Courage, "Expert judgment in life-cycle degradation and maintenance modelling for steel bridges," *Life-Cycle Eng. Syst. Emphas. Sustain. Civ. Infrastruct. - 5th Int. Symp. Life-Cycle Eng. IALCCE 2016*, pp. 2130–2137, 2017, doi: 10.1201/9781315375175-313.

[89] MathWorks, "Copula random numbers." 2006, [Online]. Available: https://www.mathworks.com/help/stats/copularnd.html.

[90] Mathworks, "Beta inverse cumulative distribution function." 2006, [Online]. Available: https://www.mathworks.com/help/stats/betainv.html.

[91] Kullback S, Leibler RA. On information and sufficiency. Ann Math Stat 1951;22. https://doi.org/10.1214/aoms/1177729694.

[92] K. T. Abou–Moustafa, F. De La Torre, and F. P. Ferrie, "Designing a Metric for the Difference between Gaussian Densities," in *Brain, Body and Machine*, .